Discrete and nonlocal models of Engesser and Haringx elastica

Attila Kocsis, Noël Challamel, György Károlyi

Discrete and nonlocal models of Engesser and Haringx elastica

Attila Kocsis

Department of Structural Mechanics, Budapest University of Technology and Economics and Engineering Center Budapest, Robert Bosch Kft., 1111, Budapest, Hungary

Noël Challamel

Universit de Bretagne Sud, EA 4250, Institut de Recherche Dupuy de Lôme (IRDL), Centre de Recherche, Rue de Saint Maudé-BP 92116, F-56100 Lorient, France

György Károlyi

Institute of Nuclear Techniques, Budapest University of Technology and Economics, 1111 Budapest, Műegyetem rkp. 3., Hungary

Abstract

In this paper a generalized discrete elastica including both bending and shear elastic interactions is developed and its possible link with nonlocal beam continua is revealed. This lattice system can be viewed as the generalization of the Hencky bar-chain model, which can be retrieved in the case of infinite shear stiffness. The shear contribution in the discrete elastica is introduced by following the approach of Engesser (normal and shear forces are aligned with and perpendicular to the link axis, respectively) and that of Haringx (shear force is parallel to end section of links), both supported by physical arguments. The nonlinear analysis of the shearable-bendable discrete elastica under axial load is accomplished. Buckling and post-buckling of the lattice systems are analysed in a geometrically exact framework. The buckling loads of both the discrete Engesser and Haringx elastica are analytically calculated, and the post-buckling behavior is numerically studied for large displacement. Nonlocal Timoshenko-type beam models, including both bending and shear stiffness, are then built from the continualization of the discrete systems. Analytical solutions for the fundamental buckling loads of the nonlocal Engesser and Haringx elastica models are given, and their first post-buckling paths are numerically computed and compared to those of the discrete Engesser and Haringx elastica. It is shown that the nonlocal Timoshenko-type beam models efficiently capture the scale effects associated with the shearable-bendable discrete elastica.

Keywords: Lattice; Discrete elastica; Shear effect; Nonlocal beam mechanics; Timoshenko beam elements; Scale effect; Buckling; Bifurcation; Post-buckling; Finite Difference Methods

1. Introduction

In this paper the possible link between discrete beam systems and their continuum analogies for structural mechanics applications is investigated. One related question is whether we can build nonlocal beam models from discrete systems composed of rigid elements linked by concentrated or distributed interaction. A pioneer model for relating discrete beam mechanics with its continuum analogue is the so-called *Hencky*

bar-chain model, which is composed of rigid elements connected by concentrated rotational springs (*Hencky* [1]). *Hencky* [1] considered this lattice system for estimating the buckling load of the *Euler-Bernoulli* beam (*Euler* [2]). *Hencky* [1] presented some solutions for small number of links, namely $n = 2$, 3 and 4, and showed the efficiency of this computation method for approximating the buckling load of the continuous *Euler-Bernoulli* beam. The exact buckling load valid for any number of links was derived by *Wang* [3, 4] by solving a linear, discrete boundary value problem. In fact, as pointed out by *Silverman* [5], the difference equations of *Hencky* bar-chain model are the central finite difference formulation of the continuous *Euler-Bernoulli* beam equations. This strong connection between lattice mechanics and finite difference method was also discussed by *Maugin* [6] and *Challamel et al* [7]. It is worth mentioning that alternative lattice models with distributed microstructure can be related to the finite element method, as recently studied by *Kocsis and Challamel* [8]. Going back to *Hencky*'s model and due to the interest of the mechanics community in understanding the discretization properties of nonlinear systems, the post-buckling behavior of *Hencky* bar-chain model was reconsidered in the 80s independently by *El Naschie et al* [9] and *Gáspár and Domokos* [10]. *Gáspár and Domokos* [10], *Domokos* [11], *Domokos and Holmes* [12] *Károlyi and Domokos* [13], and *Kapsza et al* [14] revealed how rich and complex equilibrium states the *Hencky* bar-chain model can possess, contrary to the *Bernoulli-Euler* beam. This complex behavior is because of the discrete system is spatially chaotic as pointed out by *Domokos and Holmes* [12]. In fact, the discrete *Hencky* bar-chain model shows spatial chaotic behavior not only if axially compressed and simply supported, but also under different (even non-conservative) loadings and boundary conditions (see *Kocsis and Károlyi* [15, 16] and *Kocsis* [17]). Discrete microstructured systems with both shear and bending effects were considered for instance by *Ostoja-Starzewski* [18], *Zhang et al* [19] and *Duan et al* [20] in different physical systems. *Ostoja-Starzewski* presented results for dumbbell particles (vertical rigid bars) of X-braced girder geometry, whereas *Zhang et al* [19] and *Duan et al* [20] used generalized *Hencky*-type systems with bending-shear interaction for buckling (*Zhang et al* [19]) and vibrations behavior (*Duan et al* [20], respectively). Recently, *Dell'Isola et al* [21] has investigated the behavior of a pantographic sheet or pantographic lattice composed of extensionable springs with concentrated rotational stiffnesses. This two-dimensional lattice can be viewed as a possible two-dimensional generalization of *Hencky*'s system with an extensibility condition for each cell Lattice beam models have a wide range of applications ranging from stability in construction engineering [22], through computer graphics and image analysis [23] to nanostructures [24] and biomechanics [25]. As an example for biomechanical application, a 3D discrete model was developed by *Coleman et al* [25] for studying sequence-dependent DNA elasticity, while the 2D counterpart of this model, the discrete planar *Cosserat* rod was developed by *Kocsis* [26].

The discrete elastica problem has been recently revisited from a nonlocal point of view by *Challamel et al* [27], who showed the efficiency of nonlocal mechanics to capture the scale effects of the discrete elastica. The nonlocal beam model considered by *Challamel et al* [27] was built by continualization of the governing difference equations of the discrete elastica, leading to an equivalent stress gradient model (as used by *Eringen* [28] for axial lattice dynamics). They [27] also showed that the nonlocal terms of the nonlocal continualized beam model strongly depend on the lattice spacing of *Hencky* bar-chain model. The continualization method used in *Challamel et al* [27] implemented stress gradient operators, but strain gradient operators can also be used for other continuous approximations of the discrete problem (*Challamel et al* [29]). In other words, nonlocal *Euler-Bernoulli* beam model can be built from *Hencky* bar-chain model by using a continualization method, both in the linear and in the nonlinear range.

The present paper generalizes these results by including the effect of shear deformation. The influence of

the shear effect in the buckling of local continuous columns can be introduced through two different theories, the *Engesser* theory [44] and the *Haringx* theory [30]. These theories differ in the normal and shear force definitions, which can be defined with respect to the non-deformed or the deformed cross-section. In the case of the *Engesser* theory, the normal force is chosen to be parallel to the deformed beam axis, whereas in the *Haringx* approach the normal force is chosen to be normal to the cross-section. The differences between these shear theories can be understood as a difference of strain measure definition, as extensively detailed by *Bažant* [31] (see more recently *Bažant and Cedolin* [32]). The buckling of extensible, shearable and bendable columns has been studied by *Ziegler* [33] for an *Engesser* based model, later generalized by *Reissner* [34] for both *Engesser* and *Haringx* based models, with energetic arguments.

The buckling of *Hencky* bar-chain model extended by some shear effects has been studied by *Zhang et al* [19], who also continualized this discrete structural model to obtain a nonlocal *Timoshenko* beam model. However, *Zhang et al* [19] only considered the linearized buckling problem and obtained an *Engesser*-type formula for the buckling load. In this paper we introduce two generalized *Hencky* bar-chain models, both of which possess bending and shear interactions. One model turns out to be a lattice system corresponding to the *Engesser* elastica, while the other model is a lattice system corresponding to the *Haringx* elastica. Geometrically exact nonlocal *Engesser* and *Haringx* elastica are then asymptotically obtained from a continualization process applied to the discrete *Haringx* and *Engesser* elastica. Nonlocal *Engesser* and *Haringx* elastica are also obtained by using *Eringen*'s nonlocal elasticity [28] for small displacements in order to verify and comprehend the continualized nonlocal models. It is shown that the continualized nonlocal models can be obtained from *Eringen*'s nonlocal elasticity if nonlocality affects only the bending, but not the shear terms of the constitutive law. Analytical solutions for the buckling loads of the introduced discrete and nonlocal models are derived and numerical solutions for the first post-buckling paths are given for the discrete and nonlocal models for large displacements. Numerically obtained bifurcation diagrams of the discrete systems are also plotted.

2. The generalized Hencky bar-chain model

The model of the generalized *Hencky* bar-chain model, a shearable-bendable elastic linkage, is shown in Figure 1 (a). There are N links connected by frictionless hinges in the x, y–plane. Initially, each link is a rectangular object, its longer side length, also called the length of the link, is a_0 parallel to the x-axis. In the unloaded state the linkage is straight, its total length is $L = N \cdot a_0$. Upon loading each link can undergo rigid–body–like rotation, and can be distorted due to *shearing*. The rigid–body–like rotation of link i is denoted by θ_i. Both the link axis and the end sections of the link rotate by this angle while the length of the link remains a_0. Then the link can be distorted such that the link axis is rotated by an additional (shear) angle γ_i, while the end sections of the link keep their angle θ_i, and the length of the link becomes a_i. The shear force that develops during distortion will be defined later, since it depends on the applied shear strain theory. The neighboring end sections of adjacent links are connected by linear rotational springs of stiffness ρ. These are called bending springs. The moment in the ith bending spring is given by the material law:

$$M_i = \rho \left(\theta_{i+1} - \theta_i \right). \tag{1}$$

Hinge 0, at the starting end of the linkage, is fixed, while hinge N is supported by a roller which

constraints translation along the y axis. Hence, the supports are at the same height, $y_0 = y_N$, leading to the kinematic boundary condition:

$$y_N - y_0 = 0. \tag{2}$$

The structure is loaded by a horizontal, compressive (axial) force P at hinge N. There are zero moments at the ends of the linkage, defining the force boundary conditions $M_0 = M_N = 0$, which, along with the discrete constitutive law Eq. (1), yield:

$$\theta_0 = \theta_1, \quad \theta_{N+1} = \theta_N. \tag{3}$$

Figure 1 (b) shows a schematic free body diagram of the displaced link i. If hinges 0 and N do not coincide, then the reaction force in the roller, and the vertical component of the reaction force in the fixed hinge are zero.

We will implement two types of shear strain theories for the links. First we follow *Timoshenko*'s finite shear strain theory [35], assuming that the shear deformation preserves the initial *length* of the link axis. Hence, after the links are distorted, their length remain constant, $a_i = a_0$. This approach is discussed in Section 3.

Then we apply *Love*'s finite shear strain theory [36], assuming that the shear deformation preserves the initial *area* of the links. In this case, the length of the ith link axis becomes $a_i = a_0/\cos\gamma_i$ after the shear deformation. This approach is detailed in Section 4.

3. Discrete and nonlocal Engesser elastica

The deformed link i, following *Timoshenko*'s finite shear strain theory, is shown in Figure 2. The length of the link is *preserved* during the shear deformation, $a_i = a_0$, while the area of the link *decreases*.

If the linkage is a discrete model of a homogeneous, prismatic beam of bending stiffness EI and shear stiffness κGA, then the stiffness of the bending springs is $\rho = EI/a_0$ and the stiffness of the shearable links is $k = \kappa GA a_0$. The total potential energy of the structure is the sum of internal and external potentials:

$$\Pi_{\text{tot}} = \frac{1}{2}\rho \sum_{i=1}^{N-1} (\theta_{i+1} - \theta_i)^2 + \frac{1}{2} k \sum_{i=1}^{N} \gamma_i^2 + P a_0 \sum_{i=1}^{N} \cos(\theta_i + \gamma_i). \tag{4}$$

The dimensionless total potential energy is obtained by dividing Eq. (4) by ρ:

$$\Pi = \frac{1}{2} \sum_{i=1}^{N-1} (\theta_{i+1} - \theta_i)^2 + \frac{\alpha}{2N^2} \sum_{i=1}^{N} \gamma_i^2 + \frac{\beta}{N^2} \sum_{i=1}^{N} \cos(\theta_i + \gamma_i) \tag{5}$$

Here the following *stiffness and load parameters* are introduced:

$$\alpha = \frac{\kappa G A L^2}{EI}, \quad \beta = \frac{P L^2}{EI}. \tag{6}$$

In an equilibrium configuration the total potential energy is stationary [37]. This condition yields the $2N$ equilibrium equations of the structure:

$$\frac{\partial \Pi}{\partial \theta_i} = -\left(\theta_{i+1} - 2\theta_i + \theta_{i-1}\right) - \frac{\beta}{N^2} \sin\left(\theta_i + \gamma_i\right) = 0, \tag{7}$$

$$\frac{\partial \Pi}{\partial \gamma_i} = \frac{\alpha}{N^2}\gamma_i - \frac{\beta}{N^2} \sin\left(\theta_i + \gamma_i\right) = 0, \quad i = 1, \ldots, N. \tag{8}$$

If Eqs. (7) are summed, and the static boundary conditions Eq. (3) are taken into account, then the kinematic boundary condition Eq. (2) is satisfied for $\beta \neq 0$.

Note the physical meaning of Eq. (7): It is the equilibrium of moments of link i. Now let us decompose the force P. The axial component, $P\cos(\theta_i + \gamma_i)$, has no apparent effect since the link is inextensible. The component perpendicular to the link axis, $P\sin(\theta_i + \gamma_i)$, shears the link, and cause the shear strain γ_i. This is meant by Eq. (8) in a non-dimensional form. Therefore, the introduced model inherits a discrete *Engesser*-type approach: the normal and shear forces are aligned with and perpendicular to the link axis, respectively [32].

By introducing

$$\Psi_i = \theta_i + \gamma_i, \tag{9}$$

the angle of the link axis, the equilibrium equation system Eqs. (7)–(8) can be written as:

$$\Psi_{i+1} - 2\Psi_i + \Psi_{i-1} - \frac{\beta}{\alpha}\left(\sin\Psi_{i+1} - 2\sin\Psi_i + \sin\Psi_{i-1}\right) + \frac{\beta}{N^2}\sin\Psi_i = 0, \quad i = 1, \ldots, N \tag{10}$$

with boundary conditions $\Psi_0 = \Psi_1$ and $\Psi_{N+1} = \Psi_N$. Note that Eq. (10) is identical to the difference equation system of *Hencky* bar-chain model as $\alpha \to \infty$, i.e. as the links become unshearable.

3.1. Buckling load of the discrete Engesser elastica

The trivial solution for Eq. (10), for fixed stiffness parameter α, is: $\Psi_i = 0$, and β is arbitrary. This solution defines the trivial equilibrium states of the structure. A *Hessian*, formed by the partial derivatives of Eq. (10) with respect to Ψ_i, around the trivial state is the following:

$$\mathbf{H} = -\mathbf{C}\left(1 - \frac{\beta}{\alpha}\right) + \frac{\beta}{N^2}\mathbf{I}. \tag{11}$$

Here $\mathbf{I}$ is the N–by–N identity matrix, while $\mathbf{C}$ is the N–by–N modified continuant matrix defined as $C_{i,i} = 2$, except for $C_{1,1} = C_{N,N} = 1$, $C_{i,i+1} = C_{i,i-1} = -1$, and zero otherwise. If at least one

eigenvalue of $\mathbf{H}$ is zero, then the trivial equilibrium state is critical, which implies that the structure may buckle [38]. An eigenvalue is zero if $\det(\mathbf{H}) = 0$, hence if $\beta/\left(N^2(1-\beta/\alpha)\right)$ is an eigenvalue of $\mathbf{C}$. The eigenvalues of $\mathbf{C}$ are

$$\lambda_i = 4\sin^2\frac{i\pi}{2N}, \quad i = 0, \dots, N-1 \tag{12}$$

(see page 232 of [39] for details). There is a trivial solution of $i = 0$ and $\beta = 0$, which implies $P = 0$ or $EI \to \infty$. The other solutions give the buckling loads of the structure:

$$\beta_{\mathrm{cr},i} = \frac{4N^2\sin^2\frac{i\pi}{2N}}{1+\dfrac{4N^2\sin^2\frac{i\pi}{2N}}{\alpha}}, \quad i = 1, \dots, N-1. \tag{13}$$

It is important to observe that all of these $N-1$ buckling loads are *compressive*, thus the structure can buckle only under compression. The fundamental buckling load of the discrete *Engesser* elastica is obtained from Eq. (13) with $i = 1$ as:

$$\beta_{\mathrm{dE}} = \frac{4N^2\sin^2\frac{\pi}{2N}}{1+\dfrac{4N^2\sin^2\frac{\pi}{2N}}{\alpha}} = \frac{\beta_{\mathrm{H}}}{1+\dfrac{\beta_{\mathrm{H}}}{\alpha}}. \tag{14}$$

Here

$$\beta_{\mathrm{H}} = 4N^2\sin^2\frac{\pi}{2N} \tag{15}$$

is the fundamental buckling load of *Hencky*'s system [4, 12, 40], to which Eq. (14) tends in the unshearable limit, i.e. as $\kappa GA \to \infty$, $\alpha \to \infty$. In view of this, the formula that has been developed for the fundamental buckling load of our shearable, bendable discrete model, Eq. (14), follows the *Föppl-Papkovich* summation pattern [41].

The *unbendable* case implies $EI \to \infty$. Then the buckling load equals the shear stiffness of the structures, which corresponds to the elastic web of links [17, 42], a discrete model of *Timoshenko*'s unbendable, inextensible, but shearable column [35].

Note that Eq. (15) has already been given by *Zhang et al* [19], corresponding to a different micromechanical model of the nonlocal *Timoshenko* beam.

3.2. Asymptotic limit: the local Engesser elastica

In the continuum limit Eq. (10) yields the *local Engesser elastica*:

$$\frac{\mathrm{d}^2}{\mathrm{d}\xi^2}\left(\Psi - \frac{\beta}{\alpha}\sin\Psi\right) + \beta\sin\Psi = 0, \tag{16}$$

with $\xi = s/L$ being the non-dimensional arc-length parameter, $\mathrm{d}^2/\,\mathrm{d}\xi^2$ denotes the second derivative with respect to ξ, and $\Psi(\xi) = \theta(\xi) + \gamma(\xi)$. It can be also written as

$$\frac{\mathrm{d}^2\Psi}{\mathrm{d}\xi^2}\left(1 - \frac{\beta}{\alpha}\cos\Psi\right) + \beta\left(1 + \frac{1}{\alpha}\left(\frac{\mathrm{d}\Psi}{\mathrm{d}\xi}\right)^2\right)\sin\Psi = 0, \tag{17}$$

which is similar to the so-called *Timoshenko* elastica equation given by *Atanackovic* [43] (see Eq. (3.3.57) on page 131).

The solution of the linearized version of Eq. (16) is

$$\Psi(\xi) = A\sin\left(\sqrt{\frac{\beta}{1-\beta/\alpha}}\xi\right) + B\cos\left(\sqrt{\frac{\beta}{1-\beta/\alpha}}\xi\right). \tag{18}$$

Satisfying pinned-pinned boundary conditions, $\Psi'(0) = \Psi'(1) = 0$, yields infinitely many buckling load parameters:

$$\beta_{\mathrm{lE},r} = \frac{r^2\pi^2}{1 + \frac{r^2\pi^2}{\alpha}}, \quad r = 1, 2, \ldots. \tag{19}$$

The fundamental buckling load of the local *Engesser* elastica is Eq. (19) at $r = 1$:

$$\beta_{\mathrm{lE}} = \frac{\pi^2}{1 + \dfrac{\pi^2}{\alpha}}, \tag{20}$$

or, in a dimensional form,

$$P_{\mathrm{lE}} = \frac{P_{\mathrm{E}}}{1 + \dfrac{P_{\mathrm{E}}}{\kappa GA}} \tag{21}$$

with $P_{\mathrm{E}} = \pi^2 EI/L^2$ being *Euler*'s formula. Note that Eq. (21) is the critical force proposed by *Engesser* [32, 44] for the buckling load of a shearable and flexural column with pinned ends. Hence, Eq. (14) is a discrete version of the *Engesser* formula.

3.3. Geometrically exact continualized nonlocal Engesser elastica

Let us introduce the rotation field $\Psi(\xi)$ of non-dimensional coordinate $\xi = x/L$ and write its *Taylor* expansion [45]:

$$\Psi\left(\xi+\frac{1}{N}\right)=\sum_{k=0}^{\infty}\frac{\frac{\mathrm{d}^k}{\mathrm{d}\xi^k}\Psi(\xi)}{k!}\left(\frac{1}{N}\right)^k=e^{\frac{1}{N}\frac{\mathrm{d}}{\mathrm{d}\xi}}\Psi(\xi). \tag{22}$$

Then the following identity can be written:

$$\begin{aligned}\Psi_{i+1}-2\Psi_i+\Psi_{i-1}&=\Psi\left(\xi+\frac{1}{N}\right)-2\Psi(\xi)+\Psi\left(\xi-\frac{1}{N}\right)\\&=4\sinh^2\left(\frac{1}{2N}\frac{\mathrm{d}}{\mathrm{d}\xi}\right)\Psi(\xi)\approx\frac{1}{N^2}\cdot\frac{\frac{\mathrm{d}^2}{\mathrm{d}\xi^2}}{1-\frac{1}{12N^2}\frac{\mathrm{d}^2}{\mathrm{d}\xi^2}}\Psi(\xi)\end{aligned} \tag{23}$$

using a Padé approximant of order [2,2]. Similarly,

$$\sin\Psi_{i+1}-2\sin\Psi_i+\sin\Psi_{i-1}=4\sinh^2\left(\frac{1}{2N}\frac{\mathrm{d}}{\mathrm{d}\xi}\right)(\sin\Psi(\xi))\approx\frac{1}{N^2}\cdot\frac{\frac{\mathrm{d}^2}{\mathrm{d}\xi^2}}{1-\frac{1}{12N^2}\frac{\mathrm{d}^2}{\mathrm{d}\xi^2}}\sin\Psi(\xi). \tag{24}$$

Then the geometrically exact differential equation of the continualized nonlocal *Engesser* elastica yields:

$$\frac{\mathrm{d}^2\Psi}{\mathrm{d}\xi^2}+\beta\sin\Psi-\beta\left(\frac{1}{\alpha}+\frac{1}{12N^2}\right)\frac{\mathrm{d}^2}{\mathrm{d}\xi^2}(\sin\Psi)=0. \tag{25}$$

This equation shows that the nonlocal effect is added to the shear effect in the nonlocal elastica. The symmetrical roles played by the shear effect and the nonlocal parameter in the shear buckling equations have been already outlined in [46].

Now analytical solution for the geometrically exact continualized nonlocal *Engesser* elastica is derived. We follow the work of *Lembo* [47], who developed analytical solutions for the nonlocal *Euler-Bernoulli* elastica for large displacements using elliptic integrals. The methodology is the same for the nonlocal *Engesser* elastica investigated in this paper. Let us introduce

$$\frac{\mathrm{d}y^*}{\mathrm{d}\xi}=\sin\Psi \tag{26}$$

and rewrite Eq. (25) as:

$$\frac{\mathrm{d}^2\Psi}{\mathrm{d}\xi^2}+\beta\frac{\mathrm{d}y^*}{\mathrm{d}\xi}-\beta\left(\frac{1}{\alpha}+\frac{1}{12N^2}\right)\frac{\mathrm{d}^3y^*}{\mathrm{d}\xi^3}=0. \tag{27}$$

Integrating the above equation once one obtains

$$\frac{\mathrm{d}\Psi}{\mathrm{d}\xi}+\beta y^*-\beta\left(\frac{1}{\alpha}+\frac{1}{12N^2}\right)\frac{\mathrm{d}^2y^*}{\mathrm{d}\xi^2}=C_1 \tag{28}$$

with C_1 being an arbitrary constant. Multiplying Eq. (28) with (26) yields

$$\frac{\mathrm{d}\Psi}{\mathrm{d}\xi}\sin\Psi+\beta y^*\frac{\mathrm{d}y^*}{\mathrm{d}\xi}-\beta\left(\frac{1}{\alpha}+\frac{1}{12N^2}\right)\frac{\mathrm{d}^2y^*}{\mathrm{d}\xi^2}\frac{\mathrm{d}y^*}{\mathrm{d}\xi}=C_1\frac{\mathrm{d}y^*}{\mathrm{d}\xi}, \tag{29}$$

which can be integrated as

$$-\cos\Psi+\frac{\beta}{2}(y^*)^2-\frac{\beta}{2}\left(\frac{1}{\alpha}+\frac{1}{12N^2}\right)\left(\frac{\mathrm{d}y^*}{\mathrm{d}\xi}\right)^2=C_0+C_1y^* \tag{30}$$

with C_0 being another arbitrary constant.

Note that $C_1=0$ due to the boundary condition Eq. (2). Hence, the following formula can be obtained:

$$\frac{\beta}{2}(y^*)^2-\frac{\beta}{2}\left(\frac{1}{\alpha}+\frac{1}{12N^2}\right)\left(\frac{\mathrm{d}y^*}{\mathrm{d}\xi}\right)^2=C_0+\sqrt{1-\left(\frac{\mathrm{d}y^*}{\mathrm{d}\xi}\right)^2}, \tag{31}$$

which shows that the shear effect and the nonlocal small length term play similar roles.

Differentiating Eq. (31) yields

$$\beta\left(y^*-\varepsilon^2\frac{\mathrm{d}^2y^*}{\mathrm{d}\xi^2}\right)+\frac{\frac{\mathrm{d}^2y^*}{\mathrm{d}\xi^2}}{\sqrt{1-\left(\frac{\mathrm{d}y^*}{\mathrm{d}\xi}\right)^2}}=0\quad\text{with}\quad\varepsilon^2=\frac{1}{\alpha}+\frac{1}{12N^2} \tag{32}$$

It is possible to reformulate Eq. (32), by using the complementary spatial coordinates

$$\left(\frac{\mathrm{d}x^*}{\mathrm{d}\xi}\right)^2+\left(\frac{\mathrm{d}y^*}{\mathrm{d}\xi}\right)^2=1\quad\rightarrow\quad\frac{\mathrm{d}x^*}{\mathrm{d}\xi}\frac{\mathrm{d}^2x^*}{\mathrm{d}\xi^2}+\frac{\mathrm{d}y^*}{\mathrm{d}\xi}\frac{\mathrm{d}^2y^*}{\mathrm{d}\xi^2}=0, \tag{33}$$

as

$$\frac{\mathrm{d}^2x^*}{\mathrm{d}\xi^2}\left(1+\beta\varepsilon^2\frac{\mathrm{d}x^*}{\mathrm{d}\xi}\right)=-\beta y^*\frac{\mathrm{d}y^*}{\mathrm{d}\xi}. \tag{34}$$

This equation has been obtained by *Lembo* [47] for the nonlocal shear inextensible column, i.e. for $\alpha\rightarrow\infty$ and with $\ell_c^2/L^2=1/(12N^2)$ for the nonlocal correspondence. An integration of Eq. (34) alternatively gives:

$$(y^*)^2 = \frac{2}{\beta}\left[c - \frac{\mathrm{d}x^*}{\mathrm{d}\xi}\left(1 + \frac{\beta\varepsilon^2}{2}\frac{\mathrm{d}x^*}{\mathrm{d}\xi}\right)\right]. \tag{35}$$

where c is an integration constant. It is finally possible to rewrite the differential equation in terms of x^*:

$$\left(\frac{\mathrm{d}^2x^*}{\mathrm{d}\xi^2}\right)^2 = \frac{2\beta\left[1 - \left(\frac{\mathrm{d}x^*}{\mathrm{d}\xi}\right)^2\right]}{\left(1 + \beta\varepsilon^2\frac{\mathrm{d}x^*}{\mathrm{d}\xi}\right)^2}\left[c - \frac{\mathrm{d}x^*}{\mathrm{d}\xi}\left(1 + \frac{\beta\varepsilon^2}{2}\frac{\mathrm{d}x^*}{\mathrm{d}\xi}\right)\right]. \tag{36}$$

The solution of this equation can be expressed in term of *Weierstrass*'s elliptic functions (see *Lembo* [47]). The correspondence with the solution of *Lembo* [47] is obtained from the shear and nonlocal factor:

$$\varepsilon^2 = \frac{1}{\alpha} + \hat{\ell_c}^2 \quad \text{with} \quad \hat{\ell_c}^2 = \frac{\ell_c^2}{L^2} = \frac{1}{12N^2}. \tag{37}$$

Lembo [47] considered the nonlocal Euler-Bernoulli beam asymptotically obtained from $\alpha \to \infty$.

Using Eq. (26), Eq. (28) and Eq. (31) can be equivalently written as:

$$\frac{\mathrm{d}\Psi}{\mathrm{d}\xi} = \frac{\sqrt{\left(\frac{1}{\alpha} + \frac{1}{12N^2}\right)\sin^2\Psi + \frac{2}{\beta}(C_0 + \cos\Psi)}}{\left(\frac{1}{\alpha} + \frac{1}{12N^2}\right)\cos\Psi - \frac{1}{\beta}} \tag{38}$$

which reduces to the local *Euler-Bernoulli* elastica as $\alpha \to \infty$ and $N \to \infty$:

$$\frac{\mathrm{d}\Psi}{\mathrm{d}\xi} = -\sqrt{2\beta(C_0 + \cos\Psi)}. \tag{39}$$

This equation can be solved using elliptic integrals [2], [35].

In order to derive the buckling load of the continualized nonlocal Engesser elastica, Eq. (25) can be linearized as

$$\left(1 - \beta\left(\frac{1}{\alpha} + \frac{1}{12N^2}\right)\right)\frac{\mathrm{d}^2\Psi}{\mathrm{d}\xi^2} + \beta\Psi = 0. \tag{40}$$

This equation is solved by

$$\Psi(\xi) = A\sin\left(\sqrt{\frac{\beta}{1 - \beta\left(\frac{1}{\alpha} + \frac{1}{12N^2}\right)}}\xi\right) + B\cos\left(\sqrt{\frac{\beta}{1 - \beta\left(\frac{1}{\alpha} + \frac{1}{12N^2}\right)}}\xi\right). \tag{41}$$

Satisfying pinned-pinned *local* boundary conditions, $\Psi'(0) = \Psi'(1) = 0$, yields infinitely many buckling load parameters of the continulized nonlocal *Engesser* elastica:

$$\beta_{\text{nlE},r} = \frac{\frac{r^2\pi^2}{1+\frac{r^2\pi^2}{12N^2}}}{1+\frac{r^2\pi^2}{\alpha\left(1+\frac{r^2\pi^2}{12N^2}\right)}}, \quad r = 1, 2, \dots. \tag{42}$$

The fundamental buckling load of the continualized nonlocal *Engesser* elastica is Eq. (42) at $r = 1$:

$$\beta_{\text{nlE}} = \frac{\frac{\pi^2}{1+\frac{\pi^2}{12N^2}}}{1+\frac{\pi^2}{\alpha\left(1+\frac{\pi^2}{12N^2}\right)}} = \frac{\beta_{\text{nle}}}{1+\frac{\beta_{\text{nle}}}{\alpha}}. \tag{43}$$

Here $\beta_{\text{nle}} = \pi^2/\left(1+\pi^2/(12N^2)\right)$ is the fundamental buckling load parameter of the *nonlocal elastica* [27]. In terms of dimensional quantities, the fundamental buckling load is:

$$P_{\text{nlE}} = \frac{P_{\text{nle}}}{1+\frac{P_{\text{nle}}}{\kappa GA}} \tag{44}$$

where

$$P_{\text{nle}} = \frac{EI\pi^2}{L_c^2}, \quad \text{with} \quad L_c = \sqrt{L^2+\ell_c^2\pi^2}, \quad \ell_c = \frac{a_0}{2\sqrt{3}} \tag{45}$$

is the fundamental (dimensional) buckling load of the *non-local elastica* [27]. It is important to outline that the nonlocal characteristic length, ℓ_c, of the nonlocal model is proportional to the length of a link, a_0, of the discrete model. Hence, the lattice size of the system is captured by the nonlocal model.

Note that Eq. (44) is an *Engesser*-type formula [32]. One only needs to replace *Euler*'s buckling load (i.e. the buckling load of the local *Bernoulli-Euler* beam) with the buckling load of the nonlocal elastica (which is the nonlocal *Bernoulli-Euler* beam) in *Engesser*'s famous formula to get the fundamental buckling load of the nonlocal *Engesser* elastica.

3.4. Eringen nonlocal Engesser elastica for small displacements

Wang et al [48] investigated the buckling of nonlocal *Engesser*-type columns where the nonlocal term only affects the bending part of the constitutive law. *Reddy* [49] investigated the buckling of nonlocal *Engesser*-type columns with both the bending part and the shear part being affected by the nonlocal terms. *Zhang et al* [19] presented a unified formulation of both nonlocal models and showed that a generalized *Hencky* model including some discrete shear stiffness behaves as a nonlocal *Timoshenko* column where the bending part of the constitutive law is affected by the small length terms (supporting the model of *Wang et al* [48] from a micromechanical point of view). Now we give the differential equations of the axially loaded

nonlocal *Engesser* elastica for small displacements and its buckling loads, and compare it to the buckling loads of the continualized model presented in this paper.

Let us start from the principle of virtual work for establishing the governing equations of the *Eringen* nonlocal *Engesser* column under axial compression, for small displacements:

$$\int_0^L \left[M\delta\psi' + V\delta(w' - \psi) - Pw'\delta w'\right] \,\mathrm{d}x = 0. \tag{46}$$

Here $M(x)$ and $V(x)$ are the internal bending moment and shear force, respectively. The translation perpendicular to the line of action of the compressive force P is denoted by $w(x)$, and the rotation of the cross-section is $\psi(x)$. The shear deformation is $\gamma(x) = w'(x) - \psi(x)$. The equilibrium equations can be written as:

$$M' + V = 0, \quad V' = Pw'' \quad \rightarrow \quad M'' = -Pw'', \quad V'' = Pw'''. \tag{47}$$

The column is incompressible, the nonlocal (stress gradient) material law is:

$$\begin{aligned} M - \ell_1^2 M'' &= EI\psi', \\ V - \ell_2^2 V'' &= \kappa GA(w' - \psi). \end{aligned} \tag{48}$$

Note that the nonlocal characteristic lengths, ℓ_1 and ℓ_2, are different for bending and shearing.

Substituting Eq. (47) in (48) yields the internal forces in terms of the kinematic variables,

$$\begin{aligned} M &= EI\psi' - P\ell_1^2 w'', \\ V &= \kappa GA(w' - \psi) + P\ell_2^2 w''', \end{aligned} \tag{49}$$

which can be substituted back in Eq. (48), yielding

$$\begin{aligned} &EI\psi'' - P\ell_1^2 w''' + \kappa GA(w' - \psi) + P\ell_2^2 w''' = 0, \\ &\kappa GA(w'' - \psi') + P\ell_2^2 w^{(4)} - Pw'' = 0. \end{aligned} \tag{50}$$

It is equivalent to the results of *Zhang et al* [19].

It is possible to express the above coupled differential equations as a sixth-order differential equation for $\hat{w}(\xi) = w(x)|_{x=\xi L}/L$. In a non-dimensional form it is:

$$\frac{\beta}{\alpha}\hat{\ell}_2^2 \hat{w}^{(6)} + \hat{w}^{(4)}\left(1 - \beta\left(\frac{1}{\alpha} + \hat{\ell}_1^2\right)\right) + \beta\hat{w}'' = 0. \tag{51}$$

Here α and β are defined by Eq. (6), while $\hat{\ell}_1 = \ell_1/L$, and $\hat{\ell}_2 = \ell_2/L$.

If it is assumed that nonlocality only affects bending, i.e. $\ell_2 = 0$, as proposed by *Wang et al* [48], then Eq. (51) reduces to a fourth-order differential equation which is solved by

$$\hat{w}(\xi) = A\cos\left(\sqrt{\frac{\beta}{1-\beta\left(\frac{1}{\alpha}+\hat{\ell}_1^2\right)}}\xi\right) + B\sin\left(\sqrt{\frac{\beta}{1-\beta\left(\frac{1}{\alpha}+\hat{\ell}_1^2\right)}}\xi\right). \tag{52}$$

For simply supported columns the associated *local* boundary conditions are $\hat{w}''(0) = \hat{w}''(1) = 0$, and the fundamental buckling load is the same as Eq. (43) if $\hat{\ell}_1 = \hat{\ell}_c = 1/(2\sqrt{3}N)$. It coincides with the results of *Wang et al* [48] and *Zhang et al* [19]. Note that the fourth-order differential equation (Eq. (51) with $\ell_2 = 0$) coincides with the second-order derivative of the linearized version of the continualized *Engesser* elastica Eq. (25), obtained from the discrete *Engesser* model for specific length scales.

Now we can state that the introduced micromechanical model, the discrete *Engesser* elastica can be associated with a stress gradient elasticity model where the nonlocality affects only the material law for bending, but not for shearing. The fundamental buckling loads of the discrete model, its continualized counterpart (the continualized nonlocal *Engesser* elastica), and the *Eringen* nonlocal *Engesser* elastica are all given by *Engesser*-type formulae.

The fundamental buckling load of the discrete *Engesser* elastica is compared to that of the nonlocal *Engesser* elastica in Table 1 for different values of N and α. The buckling load of *Hencky* bar-chain model is also given for completeness. Note that the convergence to the local solution as N increases is faster for linkages with lower shear stiffness.

3.5. Numerical solutions of the discrete and nonlocal Engesser elastica

In this section first numerical solutions are given for the first post-buckling path of the discrete and nonlocal *Engesser* elastica for some smaller values of N, and then bifurcation diagrams of the discrete *Engesser* elastica of a few links are plotted.

Figure 3 shows the first post-buckling path of the discrete *Engesser* elastica and that of the geometrically exact continualized nonlocal *Engesser* elastica for different values of N and α. The numerical solutions are obtained by using the simplex algorithm [50] as follows.

For the discrete *Engesser* elastica the difference equation system Eq. (10) was solved. For fixed number of links N there are N equations to solve, given by Eq. (10), with the boundary conditions $\Psi_0 = \Psi_1$ and $\Psi_{N+1} = \Psi_N$. The deviation of these differences from zero are the errors that are minimized by the algorithm. The unknowns of the equation system are the angles $\Psi_1, \Psi_2, \cdots, \Psi_N$ and the load parameter β (the stiffness parameter α is fixed). Hence, equilibrium paths in the $\Psi_{1\ldots N} - \beta$ space are obtained as solutions of the simplex algorithm [50]. The first post-buckling path, starting from the first bifurcation point of the trivial equilibrium branch, was followed and the projection of the path to the $\Psi_1 - \beta$ plane is shown in Figure 3 in black color.

For the nonlocal model, introducing the auxiliary variable κ, the nonlinear, second-order differential equation (25) is written in two nonlinear, first order differential equations:

$$\begin{aligned}\Psi' &= \kappa,\\ \kappa' &= \frac{\beta \sin\Psi \left(1+\kappa^2\left(\frac{1}{\alpha}+\frac{1}{12N^2}\right)\right)}{\beta\cos\Psi\left(\frac{1}{\alpha}+\frac{1}{12N^2}\right)-1}.\end{aligned} \tag{53}$$

Using *local boundary conditions*, $\kappa(0) = \kappa(1) = 0$, the equation system can be solved with the shooting method as follows. Satisfying the close-end boundary condition $\kappa(0) = 0$, the far-end boundary condition $\kappa(1)$ can be numerically computed as for an initial value problem (IVP), if some value for $\Psi(0)$ is set. For solving the differential equation system (53) as an IVP, a predictor corrector method was used. The differential equation system was discretized and the non-dimensional spatial variable ξ was divided in 1000 equal parts. Starting with $\kappa_0 = \kappa(0) = 0$ and $\Psi_0 = \Psi(0)$, the values of $\kappa_i = \kappa(i/1000)$ and $\Psi_i = \Psi(i/1000)$ were predicted by the (explicit) *Euler* method and corrected by the *Adams-Moulton* method [51]. This scheme was embedded in the path-following simplex algorithm [50]. The two unknowns of the algorithm are the angle $\Psi(0)$ and the load parameter β (the stiffness parameter α is fixed). The error function of the algorithm is the value of $\kappa(1)$. This scheme hence also yields equilibrium paths as solution. The first post-buckling path was followed starting from the first bifurcation point of the trivial equilibrium branch. The result is shown in Figure 3 in gray color.

The numerically computed fundamental buckling loads correspond to the analytical results summarized in Table 1. The first post buckling paths of the discrete and nonlocal models correlate well up to $\Psi_1 < \pi/4$. Beyond that some deviation can be observed which decreases as N increases.

The simplex algorithm is also capable to give global solutions for nonlinear boundary value problems without iterations [52]. This is done by scanning the representation space spanned by the unknowns (variables and parameter) of the problem for solutions. The drawback of the algorithm is that the required computational capacity increases exponentially with the number of unknowns. Therefore, this algorithm is applied for the discrete *Engesser* elastica of only a few links. The equations to solve and the unknowns are the same as those for the path-following process: the equations are Eq. (10) and the unknowns are $\Psi_1, \Psi_2, \ldots, \Psi_N$ and β (the stiffness parameter α is fixed). Besides, the domain of the unknowns is bounded as $\Psi_1 \in [0, \pi]$, $\Psi_{2\ldots N} \in [-2\pi, 2\pi]$, and $\beta \in [0, 150]$. Hence, only solutions found within this domain are part of the bifurcation diagram. By taking into account the symmetries of the solutions for Eq. (10), namely $\beta \to (-\beta)^k$ and $\Psi_i \to -\Psi_i + k\pi$ with $k = 1, 2, 3, \ldots$, the bifurcation diagram is derived and plotted also for negative load parameter values, $\beta \in [-150, 150]$. In order to smoothen the obtained equilibrium paths a *Newton-Raphson* iteration was applied on the results of the scanning algorithm. The solutions, i.e. bifurcation diagrams of the discrete *Engesser* elastica, are shown in Figure 4, 5 and 6 for link numbers $N = 2$, 3 and 4, respectively. The second-order equilibrium paths bifurcate from the trivial branch. They branch off the trivial equilibrium path at the buckling loads obtained analytically, given by Eq. (13) and in Table 1. Besides, there are many other equilibrium paths either bifurcating from the second-order branches (as pitchfork bifurcations), or appearing as separated branches (through saddle-node bifurcations).

The appearance of a multitude of higher order branches with the increase of beta is seminiscent of the behavior of similar spatially chaotic systems [12, 13, 14, 15, 16, 17].

4. Discrete and nonlocal Haringx elastica

A deformed link of the discrete model (Figure 1 (a)), following *Love*'s finite shear strain theory [36], is shown in Figure 7. The area of the link is preserved during the shear deformation, while its side length increases as $a_i = a_0/\cos\gamma_i$.

If the linkage is a discrete model of a homogeneous, prismatic beam of bending stiffness EI and shear stiffness κGA, then the total potential energy of the structure is:

$$\Pi_{\text{tot}} = \frac{1}{2}\rho\sum_{i=1}^{N-1}(\theta_{i+1}-\theta_i)^2 + \frac{1}{2}k\sum_{i=1}^{N}\tan^2\gamma_i + Pa_0\sum_{i=1}^{N}\frac{\cos(\theta_i+\gamma_i)}{\cos\gamma_i} \tag{54}$$

with the same bending and shear stiffness values as in Eq. (4). The dimensionless potential energy is:

$$\Pi = \frac{1}{2}\sum_{i=1}^{N-1}(\theta_{i+1}-\theta_i)^2 + \frac{\alpha}{2N^2}\sum_{i=1}^{N}\tan^2\gamma_i + \frac{\beta}{N^2}\sum_{i=1}^{N}\frac{\cos(\theta_i+\gamma_i)}{\cos\gamma_i}. \tag{55}$$

Here the stiffness and load parameters, α and β, are the same as those in Eq. (6).

The equilibrium equations of the structure are:

$$\frac{\partial\Pi}{\partial\theta_i} = -(\theta_{i+1}-2\theta_i+\theta_{i-1}) - \frac{\beta}{N^2}\frac{\sin(\theta_i+\gamma_i)}{\cos\gamma_i} = 0, \tag{56}$$

$$\frac{\partial\Pi}{\partial\gamma_i} = \frac{\alpha\tan\gamma_i - \beta\sin\theta_i}{N^2\cos^2\gamma_i} = 0, \quad i=1,\dots,N. \tag{57}$$

Summing Eqs. (56) and taking into account the static boundary conditions Eq. (3) yield the kinematic boundary condition Eq. (2) for *non–zero load*.

Similarly to the previous model, Eq. (56) is the equilibrium of moments of the ith link (see Figure 1 (b)). However, now $P\sin\theta_i$ is the shear force on link i, which is aligned with the end sections and not perpendicular to the link axis. Therefore, this discrete model follows a *Haringx*-type approach [30, 32].

The difference equation system, Eqs. (56)–(57), can be reformulated as a difference equation for the rotations θ_i, uncoupled from the shear deformation γ_i:

$$\theta_{i+1}-2\theta_i+\theta_{i-1} + \frac{\beta}{N^2}\left(1+\frac{\beta}{\alpha}\cos\theta_i\right)\sin\theta_i = 0, \quad i=1,\dots,N. \tag{58}$$

To obtain the above equation system $\tan\gamma_i = \frac{\beta}{\alpha}\sin\theta_i$ is expressed from Eq. (57) and substituted in Eq. (56) along with using the trigonometric identity $\sin(\theta_i+\gamma_i) = \sin\theta_i\cos\gamma_i + \cos\theta_i\sin\gamma_i$.

Note that Eq. (58) is the same as the difference equation system of *Hencky* bar-chain model in the unshearable limit, i.e. as $\alpha\to\infty$

4.1. Buckling load of the discrete Haringx elastica

The trivial equilibrium state of the model for fixed stiffness parameter α is defined by: $\theta_i = \gamma_i = 0$, and β is arbitrary. Around this state the *Hessian* given by the partial derivatives of Eq. (58) with respect to θ_i is:

$$\mathbf{H} = -\mathbf{C} + \frac{\beta}{N^2}\left(1 + \frac{\beta}{\alpha}\right)\mathbf{I}. \tag{59}$$

Here $\mathbf{I}$ and $\mathbf{C}$ are the same as in Section 3.1.

If the determinant of $\mathbf{H}$ is zero, $\det\left(-\mathbf{C} + \beta/N^2\,(1+\beta/\alpha)\,\mathbf{I}\right) = 0$, i.e. if $\beta/N^2\,(1+\beta/\alpha)$ is equal to an eigenvalue of the modified continuant matrix $\mathbf{C}$ (given by Eq. (12)), then the trivial equilibrium state is critical. It yields the buckling loads of the structure in the following *Haringx*-type formula:

$$\beta_{\mathrm{cr},2i-1,2i} = \frac{\alpha}{2}\left(-1 \pm \sqrt{1 + 16\frac{N^2}{\alpha}\sin^2\frac{i\pi}{2N}}\right), \quad i = 0, \ldots, N-1. \tag{60}$$

Eq. (60) at $i = 0$, with subtraction, yields a buckling load that corresponds to a *pure shear buckling mode under tension*. (Note that positive load means compression.) This is the smallest tensile buckling load, hence it is the *fundamental tensile buckling load* parameter of the discrete *Haringx* elastica:

$$\beta_{\mathrm{dH}}^{\mathrm{tens}} = -\alpha. \tag{61}$$

Hence, pure shear buckling appears in our bendable, shearable model if the shear strain follows the theory proposed by *Love*. See, for example, the discrete model of a cord [53], the discrete planar *Cosserat* rod [26], or the discrete model of DNA [54], for micromechanical models that can buckle under tension in a shear mode, or the works of *Kelly* [55], *Hodges et al* [56] and *Aristizabal-Ochoa* [57].

For each nonzero i, Eq. (60) corresponds to a *mixed buckling mode*, with one compressive and one tensile buckling load.

For the unshearable case, $\kappa GA \to \infty$, i.e. $\alpha \to \infty$, this model is also identical to the *Hencky* chain, and yields the fundamental buckling load β_{H} (see Eq. (15)). Meanwhile, for the unbendable case, $EI \to \infty$, the structure yields the discrete model of a cord [53], and undergoes pure shear buckling under *tension* at the critical load Eq. (61).

The *fundamental (compressive) buckling load* parameter of the discrete *Haringx* elastica is Eq. (60) at $i = 1$ with addition:

$$\beta_{\mathrm{dH}}^{\mathrm{comp}} = \frac{\alpha}{2}\left(\sqrt{1 + 4\frac{\beta_{\mathrm{H}}}{\alpha}} - 1\right). \tag{62}$$

4.2. Asymptotic limit: the local Haringx elastica

The local *Haringx* elastica can be asymptotically obtained from Eq. (58):

$$\frac{\mathrm{d}^2\theta}{\mathrm{d}\xi^2} + \beta\left(1 + \frac{\beta}{\alpha}\cos\theta\right)\sin\theta = 0 \tag{63}$$

with $\xi = s/L$ being the non-dimensional arc-length parameter.

The governing equations of the local *Haringx* elastica are given in the literature by *Koiter* [58], *Goto et al* [59], *Atanackovic* [43], *Huang and Kardomateas* [60], *Attard* [61] and *Humer* [62], as:

$$EI\frac{\mathrm{d}^2\hat{\theta}}{\mathrm{d}s^2} + P\sin\hat{\theta} + \frac{P^2}{\kappa GA}\sin\hat{\theta}\cos\hat{\theta} = 0, \tag{64}$$

with $\hat{\theta}(s) = \theta(\xi)|_{\xi=s/L}$. It can also be obtained from *Reissner*'s geometrically exact approach [63]. Eq. (64) is the dimensional version of Eq. (63), and hence validates that the lattice system introduced in Section 4 is a *micromechanical model of the Haringx elastica*.

The linearized version of Eq. (63) is solved by

$$\theta(\xi) = A\sin\left(\sqrt{\beta\left(1+\beta/\alpha\right)}\xi\right) + B\cos\left(\sqrt{\beta\left(1+\beta/\alpha\right)}\xi\right). \tag{65}$$

With pinned-pinned boundary conditions, $\theta'(0) = \theta'(1) = 0$, the above solution yields for the buckling load:

$$\beta\left(1+\beta/\alpha\right) = r^2\pi^2, \quad r = 0, 1, 2, \ldots. \tag{66}$$

For $r \neq 0$ critical loads corresponding to mixed (shear-bending) modes are obtained:

$$\beta_{\mathrm{lH},r} = \frac{\alpha}{2}\left(-1 \pm \sqrt{1 + 4\frac{r^2\pi^2}{\alpha}}\right), \quad r = 1, 2, \ldots. \tag{67}$$

For $r = 0$ there is a nontrivial solution, the pure shear buckling load of the local *Haringx* elastica, which is the *fundamental tensile buckling load* parameter:

$$\beta_{\mathrm{lH}}^{\mathrm{tens}} = -\alpha. \tag{68}$$

Hence, similarly to the discrete model, the (local) continuum can also buckle under tension in a pure shear mode (the axis of the buckled rod remains straight). The *fundamental (compressive) buckling load* parameter can be obtained from Eq. (67) at $r = 1$:

$$\beta_{\mathrm{lH}}^{\mathrm{comp}} = \frac{\alpha}{2}\left(\sqrt{1 + 4\frac{\pi^2}{\alpha}} - 1\right). \tag{69}$$

In a dimensional form the fundamental tensile and compressive buckling loads of the local *Haringx* elastica are:

$$P_{\mathrm{lH}}^{\mathrm{tens}} = -\kappa GA, \tag{70}$$

$$P_{\mathrm{lH}}^{\mathrm{comp}} = \frac{\kappa GA}{2}\left(\sqrt{1+4\frac{P_E}{\kappa GA}}-1\right), \tag{71}$$

with $P_{\mathrm{E}} = \pi^2 EI/L^2$ being *Euler*'s force. Note that Eq. (71) is the *Haringx* formula, the critical force proposed by *Haringx* [32, 30] originally for buckling of springs.

4.3. Geometrically exact continualized nonlocal Haringx elastica

The governing difference equation, Eq. (58), can be continualized based on Eq. (23):

$$\frac{\mathrm{d}^2\theta}{\mathrm{d}\xi^2} + \beta\left(1-\frac{1}{12N^2}\frac{\mathrm{d}^2}{\mathrm{d}\xi^2}\right)\cdot\left[\left(1+\frac{\beta}{\alpha}\cos\theta\right)\sin\theta\right] = 0, \tag{72}$$

which can be reformulated as:

$$\begin{aligned}&\left[1-\frac{\beta}{12N^2}\left(\cos\theta+\frac{\beta}{\alpha}\cos 2\theta\right)\right]\frac{\mathrm{d}^2\theta}{\mathrm{d}\xi^2} + \frac{\beta}{12N^2}\left(\sin\theta+\frac{2\beta}{\alpha}\sin 2\theta\right)\left(\frac{\mathrm{d}\theta}{\mathrm{d}\xi}\right)^2\\ &+\beta\left(\sin\theta+\frac{\beta}{2\alpha}\sin 2\theta\right)=0.\end{aligned} \tag{73}$$

No analytical solution for the geometrically exact continualized nonlocal *Haringx* elastica has been found. Next the buckling load of the continualized nonlocal *Haringx* elastica is developed.

The linearization of Eq. (72) leads to:

$$\left(1-\frac{\beta\left(1+\beta/\alpha\right)}{12N^2}\right)\frac{\mathrm{d}^2\theta}{\mathrm{d}\xi^2} + \beta\left(1+\beta/\alpha\right)\theta = 0. \tag{74}$$

The solution of this differential equation is:

$$\theta(\xi) = A\sin\left(\sqrt{\frac{\beta\left(1+\beta/\alpha\right)}{1-\frac{\beta(1+\beta/\alpha)}{12N^2}}}\xi\right) + B\cos\left(\sqrt{\frac{\beta\left(1+\beta/\alpha\right)}{1-\frac{\beta(1+\beta/\alpha)}{12N^2}}}\xi\right). \tag{75}$$

Using pinned-pinned, *local* boundary conditions, $\theta'(0) = \theta'(1) = 0$, the critical load parameters of the continualized nonlocal *Haringx* elastica can be obtained:

$$\beta_{\mathrm{nlH},r} = \frac{\alpha}{2}\left(1 \pm \sqrt{1 + 4\frac{r^2\pi^2}{\left(1+\frac{r^2\pi^2}{12N^2}\right)\alpha}}\right), \quad r = 0, 1, 2 \ldots . \tag{76}$$

For $r = 0$ a nontrivial solution exists, that is the *fundamental tensile buckling load* parameter of the nonlocal *Haringx* elastica:

$$\beta_{\mathrm{nlH}}^{\mathrm{tens}} = -\alpha. \tag{77}$$

This is the same pure shear buckling load that was derived for both the discrete and the local continuum *Haringx* elastica. This buckling load hence is the same irrespectively to the modelling scale.

Eq. (76) at $r = 1$ yields the *fundamental compressive buckling load* parameter of the nonlocal *Haringx* elastica:

$$\beta_{\mathrm{nlH}}^{\mathrm{comp}} = \frac{\alpha}{2}\left(\sqrt{1 + 4\frac{\pi^2}{\left(1+\frac{\pi^2}{12N^2}\right)\alpha}} - 1\right) = \frac{\alpha}{2}\left(\sqrt{1 + 4\frac{\beta_{\mathrm{nle}}}{\alpha}} - 1\right), \tag{78}$$

with β_{nle} being the fundamental buckling load parameter of the nonlocal elastica [27]. Note that there are infinitely many tensile and compressive buckling loads of the nonlocal *Haringx* elastica, while the discrete model has only a finite number of buckling loads.

In a dimensional form the fundamental buckling loads of the *Haringx* elastica are:

$$P_{\mathrm{nlH}}^{\mathrm{tens}} = -\kappa GA, \tag{79}$$

$$P_{\mathrm{nlH}}^{\mathrm{comp}} = \frac{\kappa GA}{2}\left(\sqrt{1 + 4\frac{P_{\mathrm{nle}}}{\kappa GA}} - 1\right). \tag{80}$$

Here P_{nle} is the fundamental buckling load of the nonlocal elastica, given already by Eq. (45).

It is worth comparing the results obtained for the local and nonlocal continuum models. The only difference is that in Eq. (71) the buckling load of the (local) *Bernoulli-Euler* beam is used in the *Haringx*-type formula, while in Eq. (80) the buckling load of the *nonlocal Bernoulli-Euler* beam appears.

4.4. Eringen nonlocal Haringx elastica for small displacements

Buckling of nonlocal *Haringx* elastica has not been presented in the literature to the best of our knowledge. Let us start from the principle of virtual work for establishing the governing equations of the axially compressed *Eringen* nonlocal *Haringx* elastica for small displacements (see for example [46]):

$$\int_0^L \left[M\delta\psi' + V\delta(w'-\psi) - Pw'\delta w' + P(w'-\psi)\delta(w'-\psi)\right]\,\mathrm{d}x = 0. \tag{81}$$

Here $M(x)$ and $V(x)$ are the internal bending moment and shear force, respectively. The equilibrium equations can be written as:

$$M' + V + P(w'-\psi) = 0, \quad V' = P\psi' \quad \rightarrow \quad M'' = -Pw'', \quad V'' = P\psi''. \tag{82}$$

The column is inextensible, the nonlocal (stress gradient) material law is given by Eq. (48). Casting Eq. (82) in (48) yields the internal forces in terms of the kinematic variables,

$$\begin{aligned} M &= EI\psi' - P\ell_1^2 w'', \\ V &= \kappa GA(w'-\psi) + P\ell_2^2\psi'', \end{aligned} \tag{83}$$

which can be substituted back in Eq. (48), yielding the coupled system of differential equations,

$$\begin{aligned} &EI\psi'' - P\ell_1^2 w''' + \kappa GA(w'-\psi) + P\ell_2^2\psi'' + P(w'-\psi) = 0, \\ &\kappa GA(w''-\psi') + P\ell_2^2\psi''' - P\psi' = 0. \end{aligned} \tag{84}$$

This differential equation system can be written as a sixth-order, non-dimensional differential equation:

$$\frac{\beta^2}{\alpha}\hat{\ell}_1^2\hat{\ell}_2^2\hat{w}^{(6)} + \left(1 - \beta\left(1+\frac{\beta}{\alpha}\right)\ell_1^2 - \frac{\beta^2}{\alpha}\ell_2^2\right)\hat{w}^{(4)} + \beta\left(1+\frac{\beta}{\alpha}\right)\hat{w}'' = 0. \tag{85}$$

Here $\hat{w}(\xi) = w(x)|_{x=\xi L}/L$, $\hat{\ell}_1 = \ell_1/L$, and $\hat{\ell}_2 = \ell_2/L$, and Eq. (6) gives α and β.

If it is assumed that nonlocality only affects bending, i.e. $\ell_2 = 0$, then Eq. (85) reduces to a fourth-order differential equation solved by:

$$\hat{w}(\xi) = A\sin\left(\sqrt{\frac{\beta\left(1+\beta/\alpha\right)}{1-\beta\left(1+\beta/\alpha\right)\ell_1^2}}\xi\right) + B\cos\left(\sqrt{\frac{\beta\left(1+\beta/\alpha\right)}{1-\beta\left(1+\beta/\alpha\right)\ell_1^2}}\xi\right). \tag{86}$$

For simply supported columns the associated boundary conditions are $\hat{w}''(0) = \hat{w}''(1) = 0$, and the same critical loads can be derived for the *Eringen* nonlocal model as for the continualized nonlocal model, Eq. (76), with $\hat{\ell}_1 = \hat{\ell}_c = 1/(2\sqrt{3}N)$.

We can conclude that the generalized *Hencky* bar-chain model, which incorporates shear deformation following *Love*'s finite strain theory, i.e. the discrete *Haringx* elastica, can be associated with a stress gradient elasticity model where the nonlocality affects only the material law for bending, but not for shearing. The

fundamental (compressive) buckling loads of the discrete model, its continualized counterpart (the continualized nonlocal *Haringx* elastica), and the *Eringen* nonlocal *Haringx* elastica are all given by *Haringx*-type formulae. All the models can *buckle under tension* in a pure shear mode, and also in mixed buckling modes. That is a feature which does not exist for the *Engesser*-type discrete and nonlocal models.

The fundamental buckling loads of the discrete *Haringx* elastica is compared to that of the nonlocal *Haringx* elastica in Table 2 for different values of N and α. The buckling load of *Hencky* bar-chain model is also included to show the buckling load in the limit when the links become unshearable. The convergence to the local solution as N increases is faster for linkages with lower shear stiffness, similarly to the *Engesser*-type models. The buckling loads of the *Engesser*-type model are lower than those of the *Haringx*-type model for the same shear stiffness parameter (see Table 1 vs. Table 2).

4.5. Numerical solutions of the discrete and nonlocal Haringx elastica

In this section some numerical solutions for the discrete and nonlocal *Haringx* elastica are given.

Figure 8 shows the first post-buckling path of the discrete *Haringx* elastica (with black line) and that of the geometrically exact continualized nonlocal *Haringx* elastica (with gray line) for different values of N and α.

For the nonlocal model the nonlinear, second-order differential equation (72) was written in the following two, nonlinear, first order differential equations:

$$\theta' = \omega, \tag{87}$$

$$\omega' = \beta \frac{\sin\theta + \frac{\beta}{2\alpha}\sin 2\theta + \frac{\omega^2}{12N^2}\left(\sin\theta + \frac{2\beta}{\alpha}\sin 2\theta\right)}{\frac{\beta}{12N^2}\left(\cos\theta + \frac{\beta}{\alpha}\cos 2\theta\right) - 1}. \tag{88}$$

Using *local boundary conditions*, $\omega'(0) = \omega'(1) = 0$, the equation system can be solved with the shooting method. A same procedure was followed as in Section 3.5.

For the results of the discrete *Haringx* elastica the difference equation system Eq. (58) was solved by the simplex algorithm [50, 52], c.f. Section 3.5. For fixed number of links N, there are N equations to solve given by Eq. (58) with boundary conditions $\theta_0 = \theta_1$ and $\theta_{N+1} = \theta_N$. The unknowns of the equation system are the angles $\theta_1, \theta_2, \cdots, \theta_N$ and the load parameter β (the stiffness parameter α is fixed). The first (compressive) post-buckling path, starting from the first bifurcation point of the trivial equilibrium branch, was followed and shown in Figure 8 in black color. This is compared to the first (compressive) post-buckling path of the nonlocal *Haringx* elastica, shown in Figure 8 in gray color. Note that in these figures the angle Ψ is used and not θ. For the nonlocal model $\Psi_1 = \Psi(0)$ is the angle of the axis tangent at $\xi = 0$.

For the discrete model bifurcation diagrams were also constructed by using the simplex algorithm, and scanning the following domain of unknowns: $\theta_1 \in [0, \pi]$, $\theta_{2\ldots N} \in [-2\pi, 2\pi]$, and $\beta \in [0, 150]$. Incorporating the symmetries of the solutions for Eq. (58), i.e. $\beta \to (-\beta)^k$ and $\Psi_i \to -\Psi_i + k\pi$ with $k = 1, 2, 3, \ldots$, the bifurcation diagram is derived and plotted also for negative load parameter values, $\beta \in [-150, 150]$. In order to smoothen the obtained equilibrium paths a *Newton-Raphson* iteration was applied on the results of the scanning algorithm. The resulting bifurcation diagrams of the discrete *Haringx* elastica of link number $N = 2$, 3 and 4 are shown in Figure 9, 10 and 11, respectively. Similarly to the bifurcation diagrams of the discrete *Engesser* elastica (Figures 4, 5 and 6), there are second-order equilibrium paths bifurcating from

the trivial branch, corresponding to Eq. (60), and also many other higher order paths either bifurcating from second-order branches (as pitchfork bifurcations), or appearing as separated branches (through saddle-node bifurcations). However, in this case bifurcations from the trivial equilibrium path occur also under tensile loads, and the secondary (post buckling) equilibrium paths in the negative load parameter regime can well be seen.

5. Conclusions

In this paper nonlocal *Engesser* and *Haringx* elastica models, including both bending and shear interactions, have been built from lattice physical systems, also called generalized *Hencky* bar-chain models. It has been shown that the nonlocality of these nonlocal beams was related to the lattice spacing of the generalized *Hencky*-type models. This connection between a bendable-shearable discrete elastica and nonlocal *Timoshenko* beam was already investigated by *Zhang et al* [19] for a linearized *Engesser*-type model. In this paper, we have introduced a different lattice system and generalized the results for geometrically exact *Engesser* and *Haringx*-type beams. Closed form solutions for the buckling loads of the lattice and nonlocal systems have been developed, and the geometrically exact nonlinear behaviour of both (*Engesser* and *Haringx*) bendable-shearable lattice systems have been also studied far beyond the buckling loads. Analytical solution for the axially compressed, pinned-pinned, geometrically exact *Engesser* elastica has been given using elliptic integrals. Numerical solutions for large displacements have been computed, bifurcation diagrams of the lattice systems have been plotted (showing higher-order equilibrium paths of the discrete models), and the first post-buckling paths of the discrete and nonlocal models have been compared. It was revealed that the *Haringx*-type models (the lattice, the nonlocal and the local, too) can buckle under tension in a pure shear mode and also in mixed flexural-shear modes. This phenomenon has an interesting aspect in a biomechanical field, namely in DNA modelling, since the molecule may undergo a shear instability under tension as was studied by *Kocsis and Swigon* [54].

In case of rigid shear interaction (infinite shear stiffness), the introduced discrete elastica systems are identical to the *Hencky* bar-chain model (see *Hencky* [1] for the linearized buckling problem, or *El Naschie et al* [9] or *Gáspár and Domokos* [10] for the post-buckling behavior). This so-called discrete elastica has been recently revisited by *Challamel et al* [27] with a nonlocal *Euler-Bernoulli* beam model, for the primary post-bifurcation branches. It has been shown that such kind of nonlocality belongs to the family of stress gradient Eringen's model [28], associated with a softening effect of the small length scale parameter. As shown in the paper, a similar nonlocality also controls the behavior of nonlocal *Engesser* and *Haringx*-type *Timoshenko* beams. The introduced model could be generalized to include extensibility, and a parallel study between a generalized *Hencky* chain with axial deformations and the extensible-elastica theory (see *Magnusson et al* [64]) could also be made.

Acknowledgement

The work of A. Kocsis was supported by the János Bolyai Research Scholarship of the Hungarian Academy of Sciences. Gy. Károlyi thanks the support from OTKA grant no. 100894.

References

References

[1] H. Hencky, Über die angenäherte Lösung von Stabilitätsproblemen im Raummittels der elastischen Gelenkkette, Der Eisenbau 11 (1920) 437–452, in German.

[2] L. Euler, Methodus inveniendi lineas curvas maximi minimive proprietate gaudentes, sive solutio problematis isoperimetrici lattissimo sensu accepti, Reprint in Opera Omnia I 24 (1744) 231–297.

[3] C. T. Wang, Discussion on the paper of "Salvadori M.G., Numerical computation of buckling loads by finite differences", Trans. ASCE 116 (1951) 629–631.

[4] C. T. Wang, Applied Elasticity, McGraw-Hill, New York, 1953.

[5] I. K. Silverman, Discussion on the paper of "Salvadori M.G., Numerical computation of buckling loads by finite differences", Trans. ASCE 116 (1951) 625–626.

[6] G. A. Maugin, Nonlinear waves in elastic crystals, Oxford University Press, 1999.

[7] N. Challamel, V. Picandet, B. Collet, T. Michelitsch, I. Elishakoff, W. C. M, Revisiting finite difference and finite element methods applied to structural mechanics within enriched continua, Eur. J. Mech. A/Solids 53 (2015) 107–120.

[8] A. Kocsis, N. Challamel, On the post-buckling of distributed microstructured system: the Finite Element elastica, International Journal of Mechanical Sciences 114 (2016) 12–20.

[9] M. S. El Naschie, C. W. Wu, A. S. Wifi, A simple discrete element method for the initial postbuckling of elastic structures, Int. J. Num. Meth. Eng. 26 (1988) 2049–2060.

[10] Z. Gáspár, G. Domokos, Global investigation of discrete models of the Euler buckling problem, Acta Technica Academiae Scientiarum Hungaricae 102 (1989) 227–238.

[11] G. Domokos, Qualitative convergence in the discrete approximation of the euler problem, Mech. Struct. Mach. 21 (4) (1993) 529–543.

[12] G. Domokos, P. Holmes, Euler's problem, Euler's method, and the standard map; or, the discrete charm of buckling, Journal of Nonlinear Science 3 (1993) 109–151.

[13] G. Károlyi, G. Domokos, Symbolic dynamics of infinite depth: finding global invariants for BVPs, Physica D 134 (1999) 316–336.

[14] E. Kapsza, G. Károlyi, S. Kovács, G. Domokos, Regular and random patterns in complex bifurcation diagrams, Discrete and Continuous Dynamical Systems 3 (2003) 519–540.

[15] A. Kocsis, G. Károlyi, Buckling under nonconservative load: conservative spatial chaos, Periodica Polytechnica Civil Engineering 49 (2005) 85–98.

[16] A. Kocsis, G. Károlyi, Conservative spatial chaos of buckled elastic linkages, Chaos 16 (2006) 033111/1–7.

[17] A. Kocsis, Spatial chaos in discrete mechanical systems: elastic linkages and elastic web of links, Ph.D. thesis, Budapest University of Technology and Economics, phD thesis in Hungarian (2008).

[18] M. Ostoja-Starzewski, Lattice models in micromechanics, Applied Mechanics Reviews 55 (1) (2002) 35–60.

[19] Z. Zhang, N. Challamel, C. M. Wang, Eringens small length scale coefficient for buckling of nonlocal Timoshenko beam based on microstructured beam model, Journal of Applied Physics 114 (2013) 114902/1–6.

[20] W. Duan, N. Challamel, C. M. Wang, Z. Ding, Development of analytical vibration solutions for microstructured beam model to calibrate length scale coefficient in nonlocal Timoshenko beams, J. Applied Physics 114 (104312) (2013) 1–11.

[21] F. Dell'Isola, I. Giorgio, M. Pawlikowski, N. L. Rizzi, Large deformations of planar extensible beams and pantographic lattices: Heuristic homogenisation, experimental and numerical examples of equilibrium, Proceedings of the Royal Society A 472 (2016) 2185.

[22] I. Hegedűs, L. P. Kollár, Structural stability in engineering practice, in: L. Kollár (Ed.), Application of the sandwich theory in the stability analysis of structures, Taylor & Francis, London, 1999, pp. 187–241.

[23] A. M. Bruckstein, R. J. Holt, A. N. Netravali, Discrete elastica, Applicable Analysis: An International Journal 78 (3–4) (2001) 453–485.

[24] Q. Wang, K. Liew, Application of nonlocal continuum mechanics to static analysis of micro- and nano-structures, Physics Letters A 363 (3) (2007) 236–242.

[25] B. D. Coleman, W. K. Olson, D. Swigon, Theory of sequence-dependent DNA elasticity, Journal of Chemical Physics 118 (2003) 7127–7140.

[26] A. Kocsis, Buckling analysis of the discrete planar cosserat rod, International Journal of Structural Stability and Dynamics 16 (3) (2016) 1450111/1–29.

[27] N. Challamel, A. Kocsis, C. M. Wang, Discrete and non-local elastica, International Journal of Nonlinear Mechanics 77 (2015) 128 – 140.

[28] A. C. Eringen, On differential equations of nonlocal elasticity and solutions of screw dislocation and surface waves, J. Appl. Phys. 54 (1983) 4703–4710.

[29] N. Challamel, A. Kocsis, C. M. Wang, Higher-order gradient elasticity models applied to geometrically nonlinear discrete systems, Theoretical and Applied Mechanics 42 (4) (2015) 223–248.

[30] J. A. Haringx, On the Buckling and Lateral Rigidity of Helical Springs, Proc. Konink. Ned. Akad. Wet. 45 (1942) 533.

[31] Z. Bažant, A correlation study of formulations of incremental deformation and stability of continuous bodies, Journal of Applied Mechanics 38 (1971) 919–928.

[32] Z. Bažant, L. Cedolin, Stability of Structures – elastic, inelastic, fracture, and damage theories, World Scientific, Singapore, 2010.

[33] H. Ziegler, Arguments for and against Engesser's buckling formulas, Ingenieur–Archiv 52 (1982) 105–113.

[34] E. Reissner, Some remarks on the problem of Euler buckling, Ingenieur–Archiv 52 (1982) 115–119.

[35] S. P. Timoshenko, J. Gere, Theory of elastic stability, McGraw-Hill, New York, 1961.

[36] A. E. H. Love, A treatise on the mathematical theory of elasticity (4th ed.), Dover Publications, New York, 1944.

[37] F. Gantmacher, Lectures in Analytical Mechanics, MIR Publishers, Moscow, 1975.

[38] A. Kocsis, An equilibrium method for the global computation of critical configurations of elastic linkages, Computers & Structures 121 (2013) 50–63.

[39] P. Rózsa, Linear Algebra and its Applications, Tankönyvkiadó, Budapest, 1991, (In Hungarian).

[40] N. Challamel, C. M. Wang, I. Elishakoff, Discrete systems behave as nonlocal structural elements: Bending, buckling and vibration analysis, European Journal of Mechanics - A 44 (2014) 125–135.

[41] T. Tarnai, Structural Stability in Engineering Practice (L Kollár Ed.), E & FN Spon, London, 1999, Ch. Summation theorems concerning critical loads of bifurcation, pp. 23–58.

[42] A. Kocsis, R. K. Németh, G. Károlyi, Spatially chaotic bifurcations of an elastic web of links, International Journal of Bifurcation and Chaos 20 (2011) 4011–4028.

[43] T. M. Atanackovic, Stability theory of elastic rods, Series on Stability, Vibration and Control of Systems, Series A: Volume 1, World Scientific, Singapore, 1997.

[44] F. Engesser, Die Knickfestigkeit gerader Stäbe, Zentralblatt der Bauverwaltung 11 (1891) 483.

[45] M. D. Greenberg, Advanced Engineering Mathematics (2nd Edition), Prentice Hall, New Jersey, 1998.

[46] N. Challamel, Higher-order shear beam theories and enriched continuum, Mechanics Research Communications 38 (2011) 388–392.

[47] M. Lembo, On nonlinear deformations of nonlocal elastic rods, Int. J. Solids Structures 90 (2016) 215–227.

[48] C. M. Wang, Y. Y. Zhang, S. S. Ramesh, S. Kitipornchai, Buckling analysis of micro- and nano-rods/tubes based on nonlocal Timoshenko beam theory, Journal of Physics D: Applied Physics 39 (7) (2006) 3904–3909.

[49] J. N. Reddy, Nonlocal theories for bending, buckling and vibration of beams, International Journal of Engineering Science 45 (2007) 288–307.

[50] G. Domokos, Z. Gáspár, A global, direct algorithm for path-following and active static control of elastic bar structures, Mechanics of Structures and Machines 23 (1995) 549–571.

[51] E. Hairer, S. P. Nørsett, G. Wanner, Solving Ordinary Differential Equations I: Nonstiff Problems, Springer-Verlag, Berlin, 1993, 2nd ed.

[52] Z. Gáspár, G. Domokos, I. Szeberényi, A parallel algorithm for the global computation of elastic bar structures, Computer Assisted Mechanics and Engineering Sciences 4 (1997) 55–68.

[53] G. Domokos, Buckling of a cord under tension, Acta Technica Hungaricae C. E. 104 (1992) 63–73.

[54] A. Kocsis, D. Swigon, DNA stretching modeled at the base pair level: Overtwisting and shear instability in elastic linkages, International Journal of Non-linear Mechanics 47 (2012) 639–654.

[55] J. M. Kelly, Tension buckling in multilayer elastomeric bearings, Journal of Engineering Mechanics 129 (12) (2003) 1363–1368.

[56] D. H. Hodges, H. Saberi, R. A. Ormiston, On tension buckling in shear-flexible composite beams, American Institute of Aeronautics and Astronautics Journal 44 (8) (2006) 1909–1911.

[57] J. D. Aristizabal-Ochoa, Tension and compression stability and second order analyses of three-dimensional multicolumn systems: effects of shear deformations, Journal of Engineering Mechanics 133 (1) (2007) 106–116.

[58] W. T. Koiter, Elastic stability of solids and structures (Ed. van der Heijden AMA), Cambridge University Press, Cambridge, 2009.

[59] Y. Goto, T. Yoshimitsu, M. Obata, Elliptic integral solutions of plane elastica with axial and shear deformations, Int. J. Solids Structures 26 (4) (1990) 375–390.

[60] H. Y. Huang, G. A. Kardomateas, Buckling and initial post-buckling behavior of sandwich beams including transverse shear, AIAA Journal 40 (11) (2002) 2331–2335.

[61] M. Attard, Finite strain-beam theory, Int. J. Solids Structures 40 (2003) 4563–4584.

[62] A. Humer, Exact solutions for the buckling and post-buckling of shear-deformable beams, Acta Mechanica 224 (2013) 1493–1525.

[63] E. Reissner, On one-dimensional finite-strain beam theory, J. Appl. Math. Phys. (ZAMP) 23 (1972) 795–804.

[64] A. Magnusson, M. Ristinmaa, C. Ljung, Behaviour of the extensible elastica solution, International Journal of Solids and Structures 38 (2001) 8441–8457.

Tables

	$N=2$		$N=3$		$N=4$		$N=5$		$N\to\infty$
	discrete	nonlocal	discrete	nonlocal	discrete	nonlocal	discrete	nonlocal	*local*
$\alpha=1$	0.88889	0.89114	0.90000	0.90043	0.90359	0.90373	0.90521	0.90526	0.90800
$\alpha=10$	4.44444	4.50137	4.73684	4.74878	4.83807	4.84192	4.88469	4.88628	4.96719
$\alpha=100$	7.40741	7.56690	8.25688	8.29322	8.56941	8.58152	8.71677	8.72185	8.98302
$\alpha=1000$	7.93651	8.11988	8.91972	8.96214	9.28555	9.29977	9.45883	9.46481	9.77315
$\alpha=10000$	7.99361	8.17966	8.99191	9.03502	9.36381	9.37827	9.54004	9.54613	9.85987
$\alpha\to\infty$	8		9		9.37258		9.54915		π^2

Table 1: Buckling loads of the discrete and nonlocal *Engesser* elastica, according to Eqs. (14) and (43), for different values of N and α. *Hencky* bar-chain model is recovered as $\alpha\to\infty$ (see Eq. (15)). The local continuum is the case of $N\to\infty$, given also by Eq. (20).

	$N=2$		$N=3$		$N=4$		$N=5$		$N\to\infty$
	discrete	nonlocal	discrete	nonlocal	discrete	nonlocal	discrete	nonlocal	*local*
$\alpha=1$	2.37228	2.40454	2.54138	2.54847	2.60203	2.60436	2.63036	2.63133	2.68113
$\alpha=10$	5.24695	5.33748	5.72381	5.74392	5.89614	5.90278	5.97686	5.97964	6.12187
$\alpha=100$	7.44563	7.60760	8.30952	8.34654	8.62814	8.64049	8.77853	8.78371	9.05049
$\alpha=1000$	7.93700	8.12041	8.92043	8.96286	9.28635	9.30057	9.45967	9.46565	9.77407
$\alpha=10000$	7.99361	8.17966	8.99191	9.03503	9.36381	9.37827	9.54005	9.54614	9.85988
$\alpha\to\infty$	8		9		9.37258		9.54915		π^2

Table 2: Fundamental (compressive) buckling loads of the discrete and nonlocal *Haringx* elastica, given by Eqs. (62) and (78), for different values of N and α. *Hencky* bar-chain model is recovered as $\alpha\to\infty$ (see Eq. (15)). The local continuum is the case of $N\to\infty$, given also by Eq. (69).

603 **Figure Captions**

Figure 1. (a) Model of the generalized *Hencky* bar-chain. The angle of the axis of link i is $\Psi_i = \theta_i + \gamma_i$, and the angle of the end sections of link i is θ_i. (b) Free body diagram of the ith link, assuming that the reaction force in the roller is zero. The moments in the bending springs are M_i and M_{i-1}, respectively.

Figure 2. Shear deformation of link i according to *Timoshenko*'s finite shear strain theory. The length of the link axis is preserved, $a_i = a_0$.

Figure 3. First post-buckling equilibrium path of the discrete *Engesser* elastica (black), which is a solution of Eq. (10), and that of the geometrically exact continualized nonlocal *Engesser* elastica (gray), which is a solution of (25), for different values of N and α. For the discrete model Ψ_1 is the angle of the first link axis, while for the nonlocal model $\Psi_1 = \Psi(0)$ is the angle of the tangent to the beam axis at $\xi = 0$.

Figure 4. Bifurcation diagram of the discrete *Engesser* elastica of $N = 2$ links, for different values of the stiffness parameter α. Numerical solutions of Eq. (10) within the domain of $\beta \in [0, 150]$, $\Psi_1 \in [0, \pi]$ and $\Psi_2 \in [-2\pi, 2\pi]$. Solutions for negative load parameter β are derived using symmetry properties.

Figure 5. Bifurcation diagram of the discrete *Engesser* elastica of $N = 3$ links, for different values of the stiffness parameter α. Numerical solutions of Eq. (10) within the domain of $\beta \in [0, 150]$, $\Psi_1 \in [0, \pi]$, $\Psi_{2...3} \in [-2\pi, 2\pi]$. Solutions for negative load parameter β are derived using symmetry properties.

Figure 6. Bifurcation diagram of the discrete *Engesser* elastica of $N = 4$ links, for different values of the stiffness parameter α. Numerical solutions of Eq. (10) within the domain of $\beta \in [0, 150]$, $\Psi_1 \in [0, \pi]$, $\Psi_{2...4} \in [-2\pi, 2\pi]$. Solutions for negative load parameter β are derived using symmetry properties.

Figure 7. Shear deformation of link i according to *Love*'s finite shear strain theory. The length of the link axis becomes $a_i = a_0/\cos\gamma_i$ while the area of the link is preserved.

Figure 8. First compressive post-buckling equilibrium path of the discrete *Haringx* elastica (black), as a solution of Eq. (58), and that of the continualized nonlocal *Haringx* elastica (gray), which is a solution of Eq. (72) for different values of N and α. For the discrete model Ψ_1 is the angle of the first link axis, but for the nonlocal model $\Psi_1 = \Psi(0)$ is the angle of the beam axis tangent at $\xi = 0$.

Figure 9. Bifurcation diagram of the discrete *Haringx* elastica of $N = 2$ links, for different values of the stiffness parameter α. Numerical solutions of Eq. (58) in the domain of $\beta \in [0, 150]$, $\theta_1 \in [0, \pi]$ and $\theta_2 \in [-2\pi, 2\pi]$. Solutions for negative load parameter β are derived using symmetry properties.

Figure 10. Bifurcation diagram of the discrete *Haringx* elastica of $N = 3$ links, for different values of the stiffness parameter α. Numerical solutions of Eq. (58) in the domain of $\beta \in [0, 150]$, $\theta_1 \in [0, \pi]$, $\theta_{2...3} \in [-2\pi, 2\pi]$. Solutions for negative load parameter β are derived using symmetry properties.

Figure 11. Bifurcation diagram of the discrete *Haringx* elastica of $N = 4$ links, for different values of the stiffness parameter α. Numerical solutions of Eq. (58) in the domain of $\beta \in [0, 150]$, $\theta_1 \in [0, \pi]$, $\theta_{2...4} \in [-2\pi, 2\pi]$. Solutions for negative load parameter β are derived using symmetry properties.

Figures

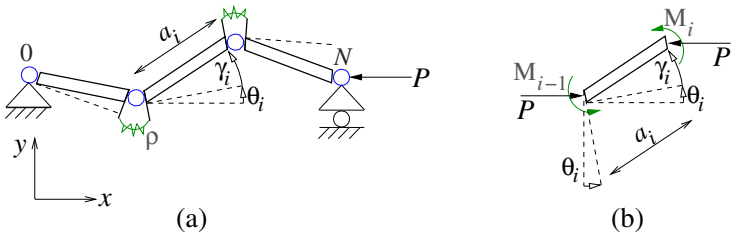

Figure 1: (a) Model of the generalized *Hencky* bar-chain. The angle of the axis of link i is $\Psi_i = \theta_i + \gamma_i$, and the angle of the end sections of link i is θ_i. (b) Free body diagram of the ith link, assuming that the reaction force in the roller is zero. The moments in the bending springs are M_i and M_{i-1}, respectively.

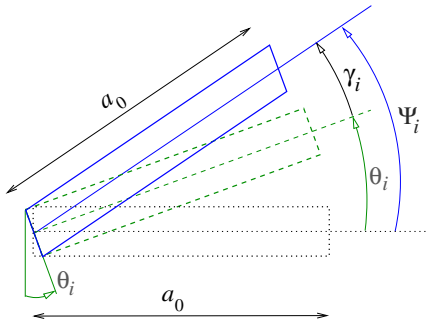

Figure 2: Shear deformation of link i according to *Timoshenko*'s finite shear strain theory. The length of the link axis is preserved, $a_i = a_0$.

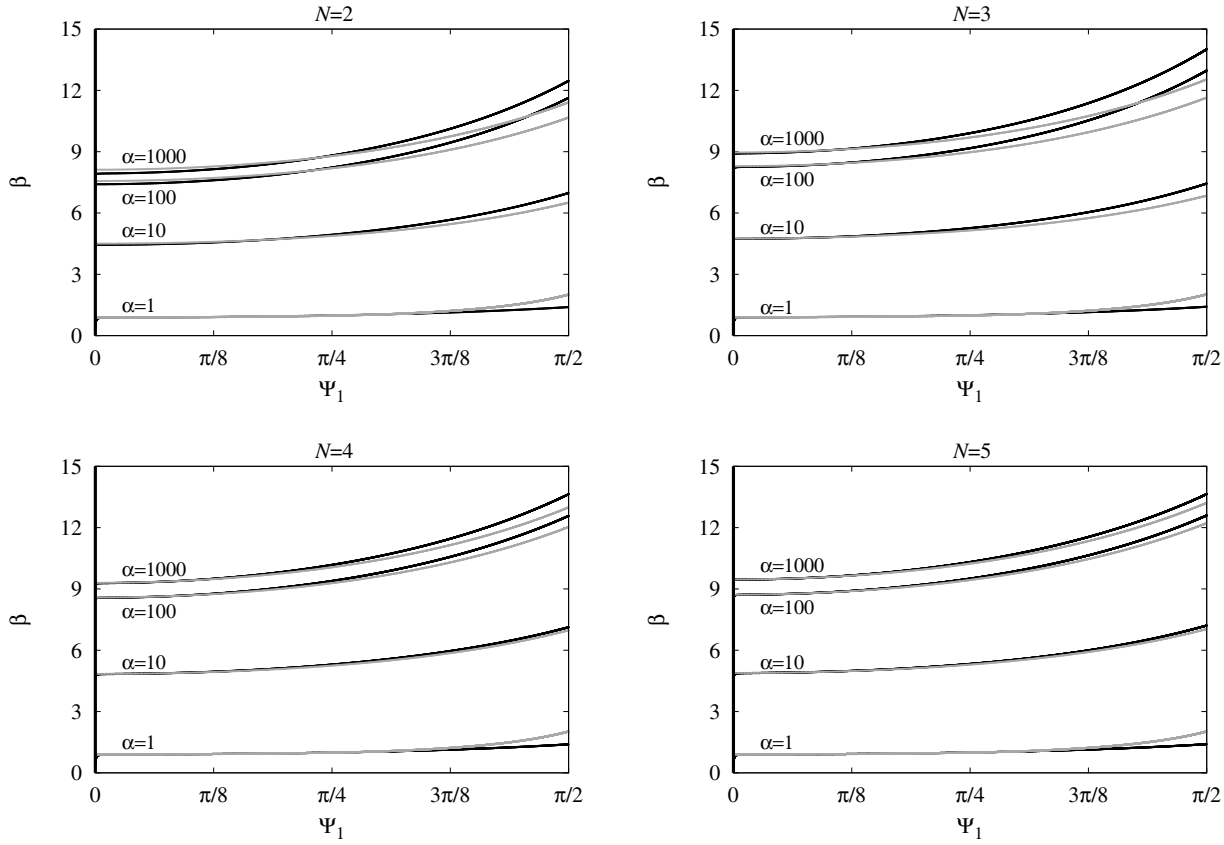

Figure 3: First post-buckling equilibrium path of the discrete *Engesser* elastica (black), which is a solution of Eq. (10), and that of the geometrically exact continualized nonlocal *Engesser* elastica (gray), which is a solution of (25), for different values of N and α. For the discrete model Ψ_1 is the angle of the first link axis, while for the nonlocal model $\Psi_1 = \Psi(0)$ is the angle of the tangent to the beam axis at $\xi = 0$.

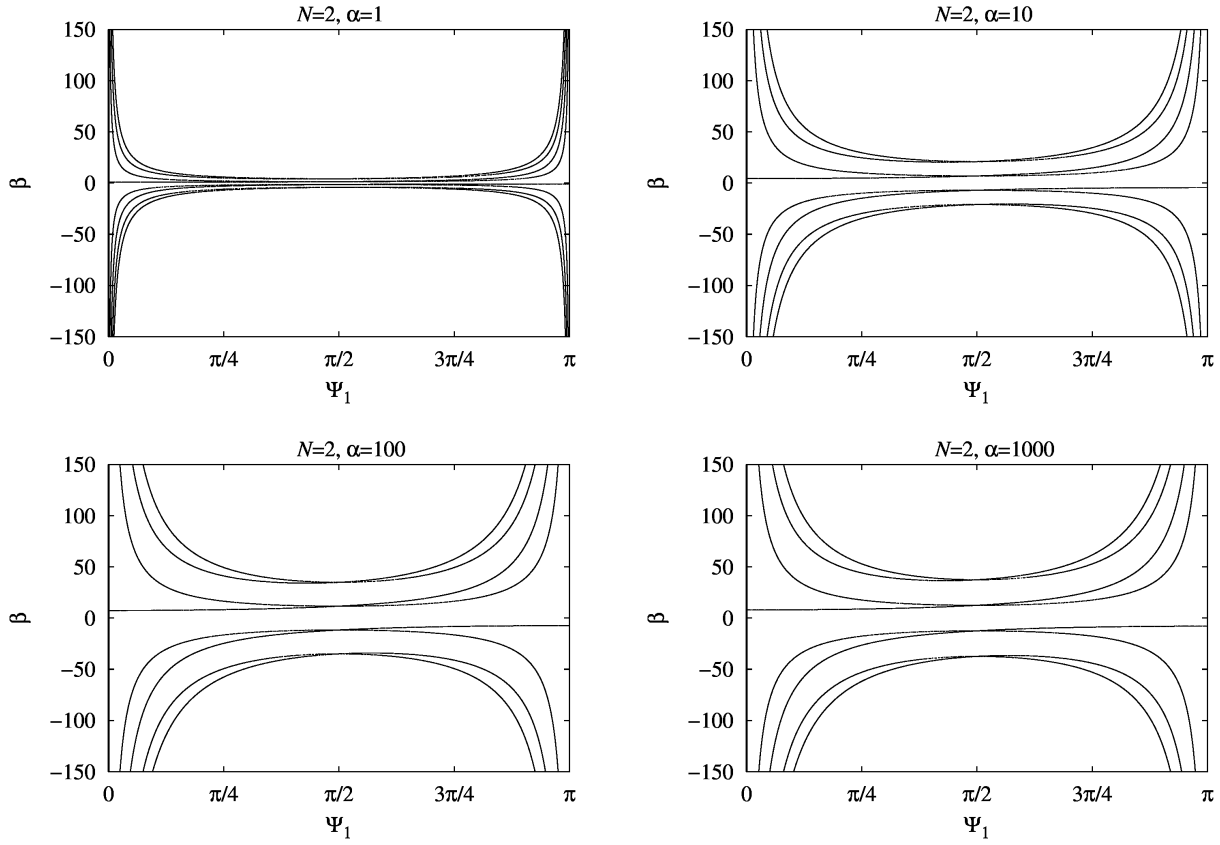

Figure 4: Bifurcation diagram of the discrete *Engesser* elastica of $N = 2$ links, for different values of the stiffness parameter α. Numerical solutions of Eq. (10) within the domain of $\beta \in [0, 150]$, $\Psi_1 \in [0, \pi]$ and $\Psi_2 \in [-2\pi, 2\pi]$. Solutions for negative load parameter β are derived using symmetry properties.

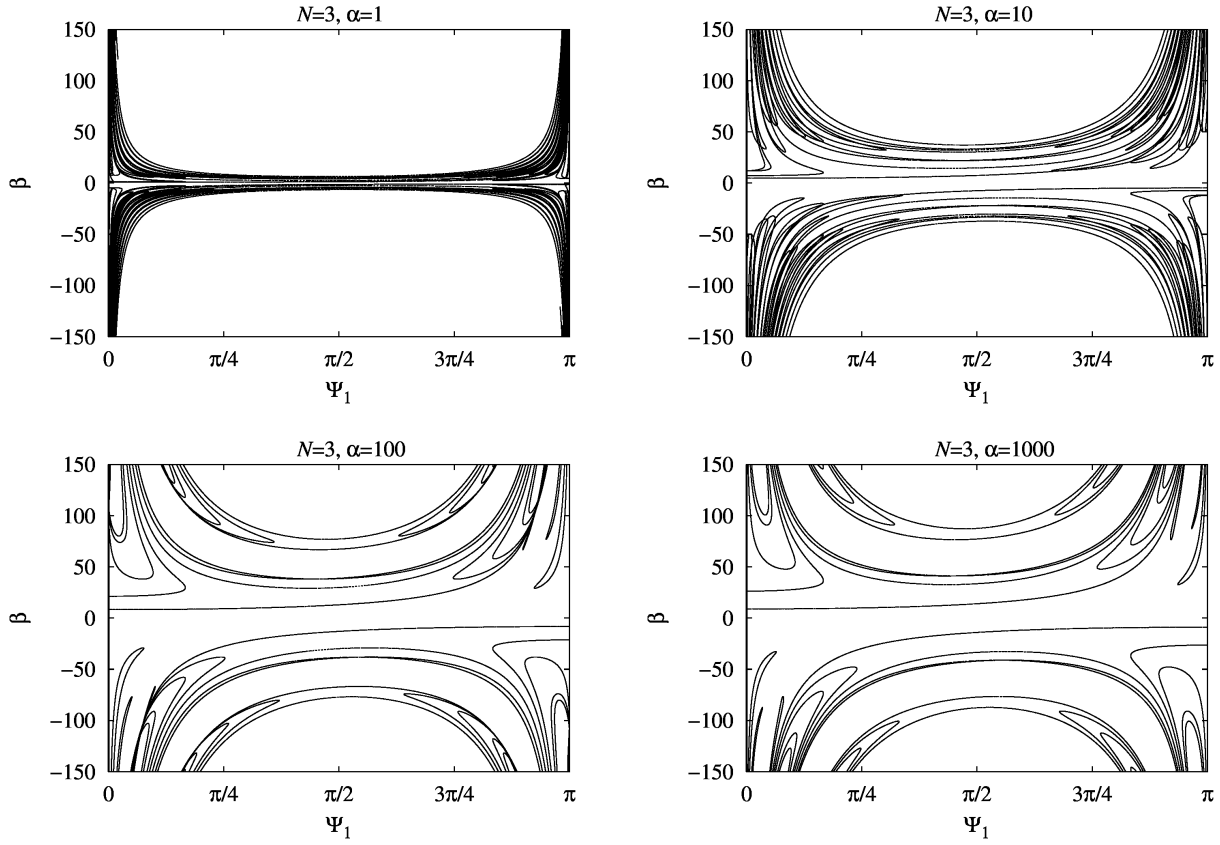

Figure 5: Bifurcation diagram of the discrete *Engesser* elastica of $N = 3$ links, for different values of the stiffness parameter α. Numerical solutions of Eq. (10) within the domain of $\beta \in [0, 150]$, $\Psi_1 \in [0, \pi]$, $\Psi_{2\ldots3} \in [-2\pi, 2\pi]$. Solutions for negative load parameter β are derived using symmetry properties.

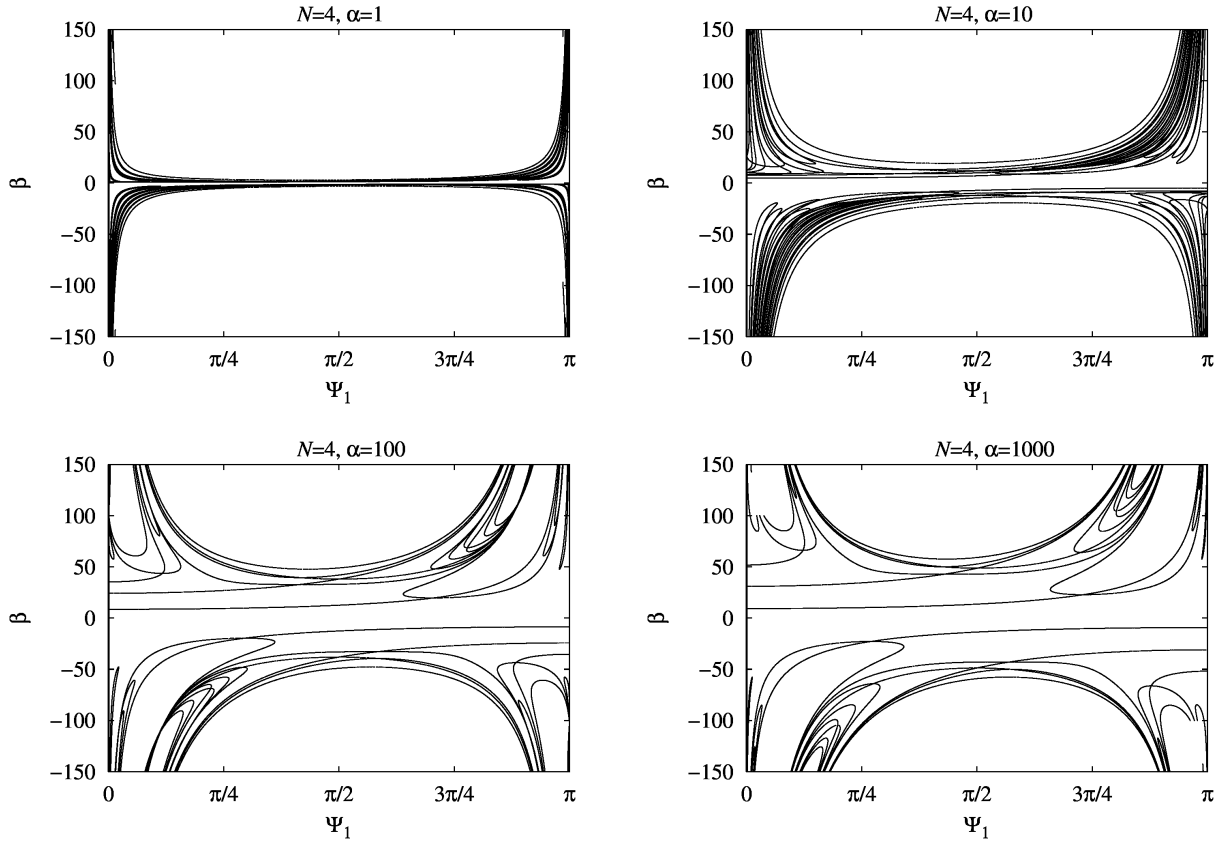

Figure 6: Bifurcation diagram of the discrete *Engesser* elastica of $N = 4$ links, for different values of the stiffness parameter α. Numerical solutions of Eq. (10) within the domain of $\beta \in [0, 150]$, $\Psi_1 \in [0, \pi]$, $\Psi_{2\ldots4} \in [-2\pi, 2\pi]$. Solutions for negative load parameter β are derived using symmetry properties.

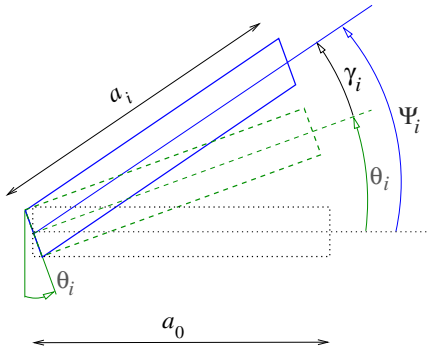

Figure 7: Shear deformation of link i according to *Love*'s finite shear strain theory. The length of the link axis becomes $a_i = a_0 / \cos\gamma_i$ while the area of the link is preserved.

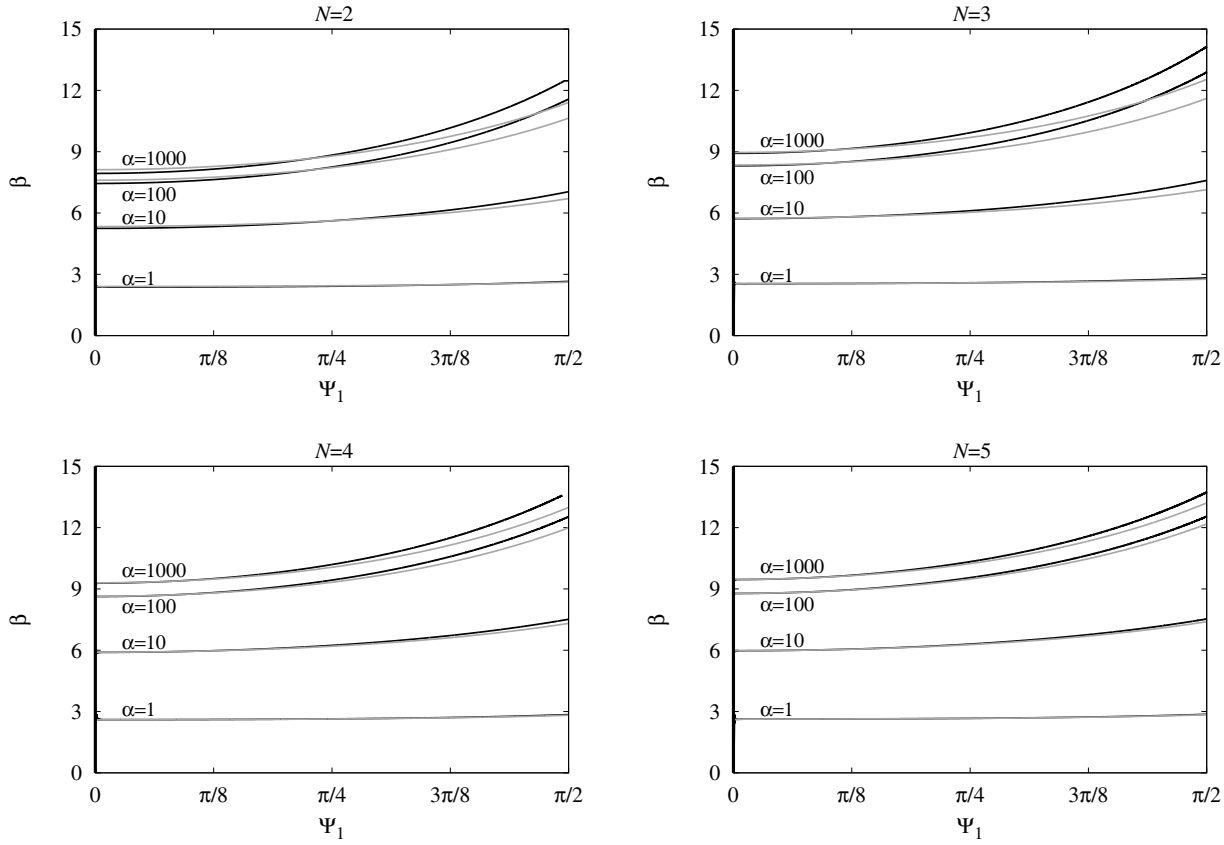

Figure 8: First compressive post-buckling equilibrium path of the discrete *Haringx* elastica (black), as a solution of Eq. (58), and that of the continualized nonlocal *Haringx* elastica (gray), which is a solution of Eq. (72) for different values of N and α. For the discrete model Ψ_1 is the angle of the first link axis, but for the nonlocal model $\Psi_1 = \Psi(0)$ is the angle of the beam axis tangent at $\xi = 0$.

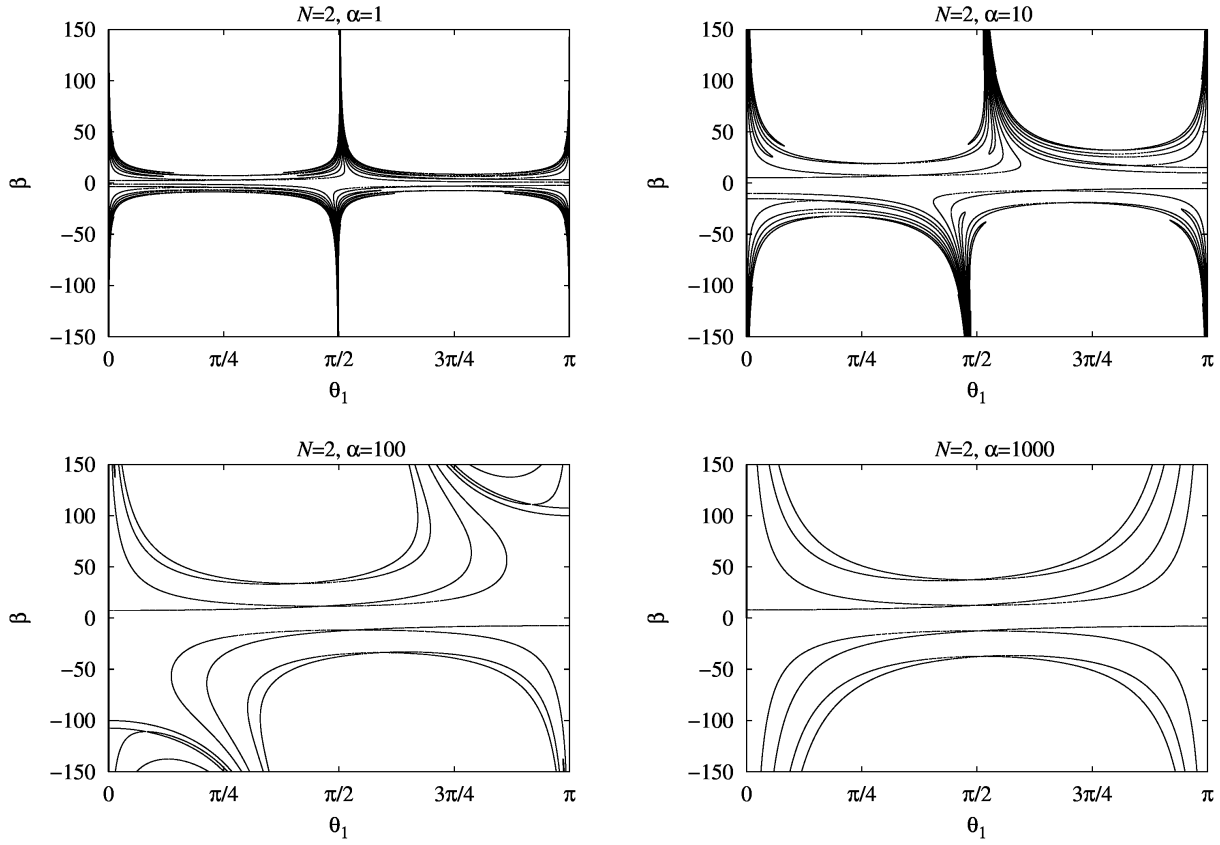

Figure 9: Bifurcation diagram of the discrete *Haringx* elastica of $N = 2$ links, for different values of the stiffness parameter α. Numerical solutions of Eq. (58) in the domain of $\beta \in [0, 150]$, $\theta_1 \in [0, \pi]$ and $\theta_2 \in [-2\pi, 2\pi]$. Solutions for negative load parameter β are derived using symmetry properties.

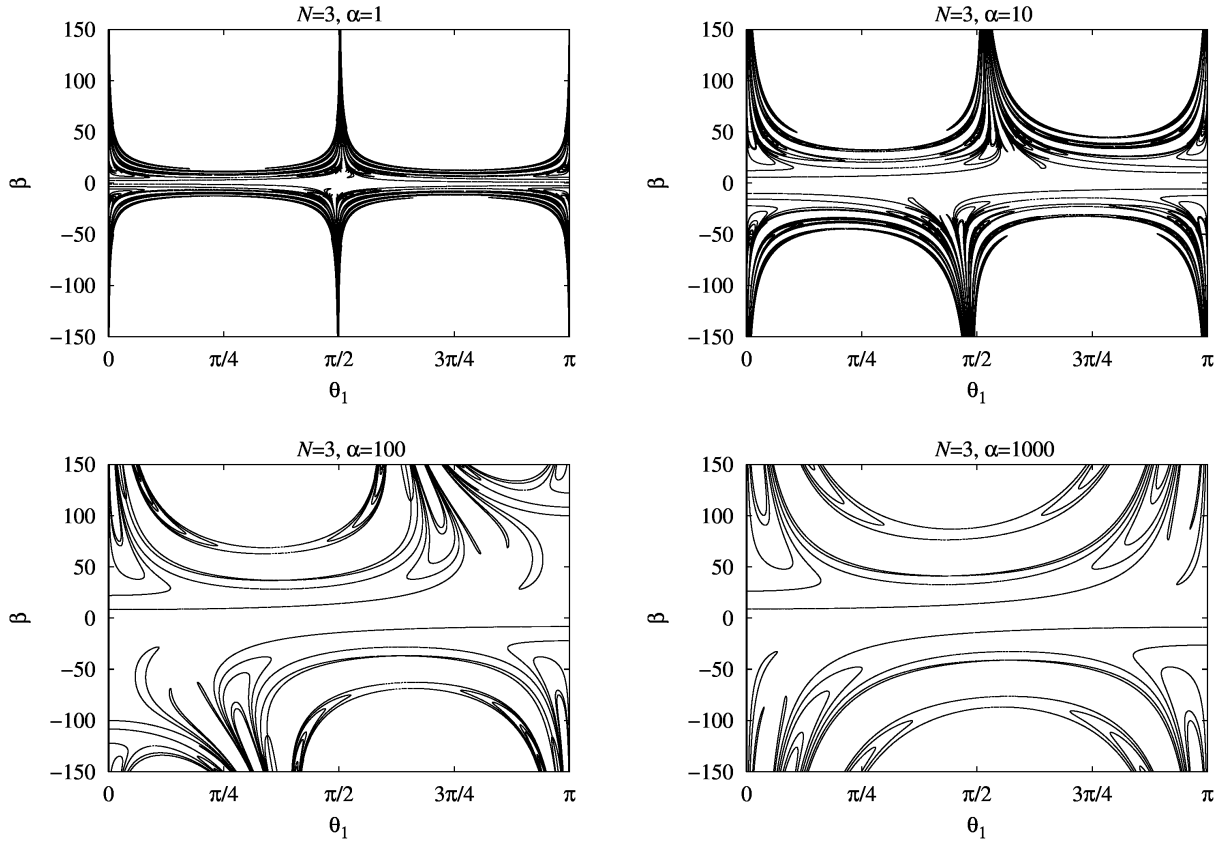

Figure 10: Bifurcation diagram of the discrete *Haringx* elastica of $N = 3$ links, for different values of the stiffness parameter α. Numerical solutions of Eq. (58) in the domain of $\beta \in [0, 150]$, $\theta_1 \in [0, \pi]$, $\theta_{2\ldots3} \in [-2\pi, 2\pi]$. Solutions for negative load parameter β are derived using symmetry properties.

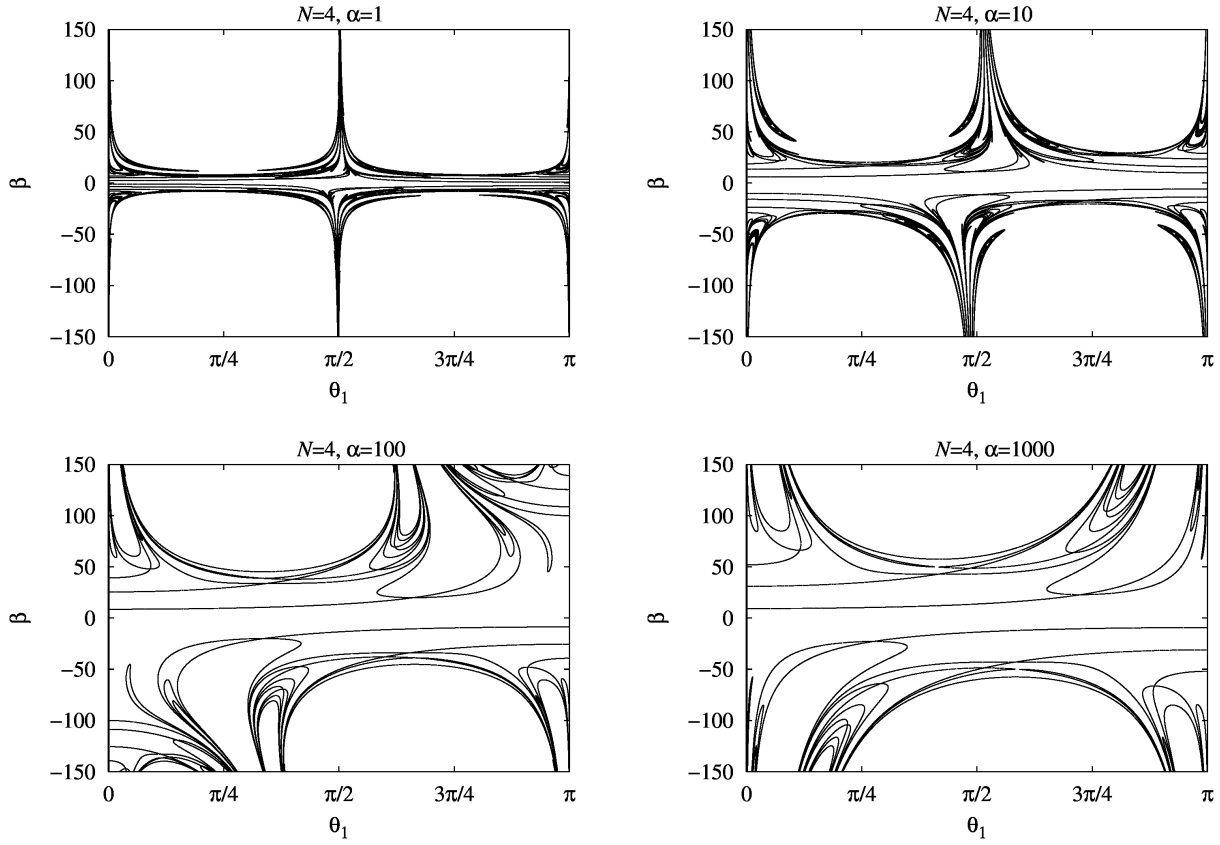

Figure 11: Bifurcation diagram of the discrete *Haringx* elastica of $N = 4$ links, for different values of the stiffness parameter α. Numerical solutions of Eq. (58) in the domain of $\beta \in [0, 150]$, $\theta_1 \in [0, \pi]$, $\theta_{2\ldots4} \in [-2\pi, 2\pi]$. Solutions for negative load parameter β are derived using symmetry properties.